

1 The furin cleavage site of SARS-CoV-2  
2 spike protein is a key determinant for  
3 transmission due to enhanced replication  
4 in airway cells.

5 Short title: SARS-CoV-2 spike cleavage and transmission

6 Authors: Thomas P. Peacock<sup>1#</sup>, Daniel H. Goldhill<sup>1#</sup>, Jie Zhou<sup>1#</sup>, Laury Baillon<sup>1#</sup>, Rebecca Frise<sup>1#</sup>, Olivia C. Swann<sup>1</sup>, Ruthiran  
7 Kugathasan<sup>1</sup>, Rebecca Penn<sup>1</sup>, Jonathan C. Brown<sup>1</sup>, Raul Y. Sanchez-David<sup>1</sup>, Luca Braga<sup>2</sup>, Maia Kavanagh Williamson<sup>3</sup>, Jack A.  
8 Hassard<sup>1</sup>, Ecco Staller<sup>1</sup>, Brian Hanley<sup>4</sup>, Michael Osborn<sup>4</sup>, Mauro Giacca<sup>2</sup>, Andrew D. Davidson<sup>3</sup>, David A. Matthews<sup>3</sup>, and  
9 Wendy S. Barclay<sup>1\*</sup>.

10 <sup>1</sup>Department of Infectious Diseases, Imperial College London, UK, W2 1PG.

11 <sup>2</sup>British Heart Foundation Centre of Research Excellence, School of Cardiovascular Medicine & Sciences, King's College  
12 London, UK, SE5 9RS

13 <sup>3</sup>School of Cellular and Molecular Medicine, Faculty of Life Sciences, University of Bristol, UK, BS8 1TD

14 <sup>4</sup>Department of Cellular Pathology, Northwest London Pathology, Imperial College London NHS Trust, UK, W6 8RF

15

16 # - these authors contributed equally to this work

17 \*Corresponding author: tel: +44 (0)20 7594 5035, email: [w.barclay@imperial.ac.uk](mailto:w.barclay@imperial.ac.uk)

18

19      Summary

20           SARS-CoV-2 enters cells via its spike glycoprotein which must be cleaved sequentially at the  
21      S1/S2, then the S2' cleavage sites (CS) to mediate membrane fusion. SARS-CoV-2 has a unique  
22      polybasic insertion at the S1/S2 CS, which we demonstrate can be cleaved by furin. Using lentiviral  
23      pseudotypes and a cell-culture adapted SARS-CoV-2 virus with a S1/S2 deletion, we show that the  
24      polybasic insertion is selected for in lung cells and primary human airway epithelial cultures but  
25      selected against in Vero E6, a cell line used for passaging SARS-CoV-2. We find this selective advantage  
26      depends on expression of the cell surface protease, TMPRSS2, that allows virus entry independent of  
27      endosomes thus avoiding antiviral IFITM proteins. SARS-CoV-2 virus lacking the S1/S2 furin CS was  
28      shed to lower titres from infected ferrets and was not transmitted to cohoused sentinel animals. Thus,  
29      the polybasic CS is a key determinant for efficient SARS-CoV-2 transmission.

30

## 31 Introduction

32 In 2019, a respiratory epidemic of unknown aetiology emerged in Hubei Province, China. The  
33 cause of the outbreak was quickly identified as a novel betacoronavirus, closely related to severe acute  
34 respiratory syndrome coronavirus (SARS-CoV) and named SARS-CoV-2 (P. Zhou et al., 2020; N. Zhu et  
35 al., 2020). SARS-CoV-2 is highly transmissible between humans and by the middle of March, the WHO  
36 declared the outbreak a pandemic (Holshue et al., 2020). It is vital to understand which molecular  
37 features of SARS-CoV-2 led to the virus causing a pandemic in order to control both the current  
38 pandemic and to prevent future coronavirus pandemics.

39 Coronaviruses enter host cells via their spike glycoprotein. Like many other enveloped virus  
40 glycoproteins, the spike protein is synthesised as a precursor that must be cleaved in order to perform  
41 its membrane fusogenic activity. Depending on the sequence of spike at the S1/S2 junction, the  
42 cleavage occurs during trafficking of spike in the producer cell by host furin-like enzymes, or by serine-  
43 proteases such as the transmembrane protease, serine 2 (TMPRSS2) at the cell surface after  
44 attachment, or by cathepsin proteases in the late endosome/lysosome (Matsuyama et al., 2010;  
45 Simmons et al., 2005). Upon cleavage of the S1/S2 junction and engagement of the host cell receptor  
46 with the spike receptor binding domain (RBD), a second cleavage site (CS) becomes exposed within  
47 the S2 domain, termed the S2' site (Belouzard, Chu, & Whittaker, 2009; Millet & Whittaker, 2014).  
48 Upon cleavage of the S2' site, generally by serine proteases or cathepsins, the S2 fusion peptide is  
49 liberated and initiates viral-host membrane fusion (Belouzard et al., 2009).

50 Like the closely related SARS-CoV, the cognate receptor of the SARS-CoV-2 spike is  
51 angiotensin-converting enzyme 2 (ACE2)(W. Li et al., 2003; P. Zhou et al., 2020). While the SARS-CoV  
52 S1/S2 junction is well characterised as being cleaved by serine proteases or cathepsins, the SARS-CoV-  
53 2 spike, similarly to the more distantly related Middle Eastern respiratory syndrome-related  
54 coronavirus (MERS-CoV), contains a polybasic CS, described as being a suboptimal furin CS (Coutard  
55 et al., 2020; Millet & Whittaker, 2014; Shang et al., 2020). This polybasic CS is absent from the closest

56 relatives of SARS-CoV-2, such as SARS-CoV, although similar polybasic CS are found in more distantly  
57 related coronaviruses (Andersen, Rambaut, Lipkin, Holmes, & Garry, 2020; Boni et al., 2020; Le  
58 Coupanec et al., 2015). It has previously been demonstrated for the MERS-CoV spike, and for SARS-  
59 CoV-2, that the furin CS at the S1/S2 junction may promote entry into lung cells (Hoffmann, Kleine-  
60 Weber, & Pohlmann, 2020; Park et al., 2016). Interestingly, SARS-CoV-2 has been shown in multiple  
61 independent studies to rapidly lose this polybasic CS upon passage in Vero E6 cells, which has been a  
62 popular cell line for isolating and propagating the virus (Davidson et al., 2020; Klimstra et al., 2020; Z.  
63 Liu et al., 2020; Ogando et al., 2020; Sasaki et al., 2020; Wong et al., 2020; Y. Zhu et al., 2020). In  
64 addition, there are reports of CS mutants isolated directly from clinical swabs (Z. Liu et al., 2020; Wong  
65 et al., 2020). Several different mutants in this region are described including total deletions of the CS,  
66 loss of arginine mutations within the CS making it less polybasic, or deletions of flanking regions  
67 leaving the polybasic tract intact but potentially affecting accessibility to protease.

68 In this study, we use a combination of lentiviral pseudotypes with spike CS mutations and Vero  
69 passaged SARS-CoV-2 virus variants to investigate the molecular mechanism by which the polybasic  
70 CS of SARS-CoV-2 mediates efficient entry into lung cells. We describe the biological consequences of  
71 these mutations and test the effect of these mutations on viral transmission in ferrets.

## 72 Results

73 The polybasic S1/S2 cleavage site of SARS-CoV-2 spike protein is cleaved by furin

74 To investigate the importance of the spike polybasic CS of SARS-CoV-2 (PRRAR), a number of  
75 spike mutants were generated which were predicted to modulate the efficiency of furin cleavage  
76 (Figure 1A) including: substituting two of the upstream arginines to produce a monobasic CS similar  
77 to SARS-CoV spike (monoCS), replacing the tribasic CS with the furin CS of a highly pathogenic H5N1  
78 avian influenza haemagglutinin containing a string of seven basic amino acids (H5CS), and two  
79 naturally occurring deletions seen following passage in Vero E6 cells and/or in clinical isolates  
80 (Davidson et al., 2020; Lau et al., 2020). The first of these removes eight amino acids including all 3

81 arginines of the PRRAR site ( $\Delta$ CS) – while the other removes five flanking amino acids but retains the  
82 tribasic site ( $\Delta$ flank). The mutations were engineered into a cDNA encoding the spike to enable cell  
83 surface expression and the generation of lentiviral pseudotypes (PV) that carry each spike variant. In  
84 addition, to study the importance of the PRRAR motif in the context of live virus we took advantage  
85 of a naturally occurring Vero cell adapted mutant SARS-CoV-2 isolate,  $\Delta$ CS (Davidson et al., 2020). This  
86 variant and the wild type virus from which it was derived were cloned by limiting dilution to enable  
87 studies using individual genotypes.

88 In several previous studies, the ability of coronavirus spike proteins to be cleaved by furin has  
89 been correlated with the ability to generate syncytia at neutral pHs when overexpressed (Belouzard  
90 et al., 2009; Hoffmann, Kleine-Weber, & Pohlmann, 2020; Xia et al., 2020). The library of SARS-CoV-2  
91 mutant spike proteins were transiently expressed in Vero E6 cells, which do not express TMPRSS2  
92 (Bertram et al., 2010; Shirato, Kawase, & Matsuyama, 2013), and syncytia formation was compared  
93 to SARS-CoV and MERS-CoV spikes (which have previously been shown to poorly and inefficiently result  
94 in syncytia formation, respectively). As described before, SARS-CoV spike expression resulted in poor  
95 syncytia formation while MERS-CoV spike produced much higher levels of syncytia (Figure 1B). SARS-  
96 CoV-2 WT spike gave an intermediate level of syncytia formation that was ablated for the mutants  
97 which were not cleaved by furin. The H5CS spike bearing the optimised furin CS produced a higher  
98 level of syncytia formation than SARS-CoV-2 WT, similar to MERS-CoV spike.

99 To investigate the differences in spike cleavage efficiency in producer cells between the  
100 mutants, we produced PV with each mutant spike protein (or SARS-CoV) in human embryonic kidney  
101 293T (293T) cells. PV were concentrated and probed by western blot (Figure 1C, left panel). Equal  
102 amounts of PV particles were loaded as indicated by p24 content. PV formed with SARS-CoV-2 WT  
103 spike had two bands reactive with anti-spike S2 antibody, corresponding to cleaved and uncleaved  
104 spike, with the stronger band corresponding to the cleaved S2 product. PV containing the H5CS spike  
105 showed very little uncleaved spike while PV with SARS-CoV WT spike and SARS-CoV-2 monobasic and

106 deletion mutants showed near compete losses of cleaved spike. When PV were produced in parallel  
107 in the presence of a furin inhibitor, full-length spike was somewhat restored for the WT and H5CS  
108 spike (Figure 1C, right panel). We also took WT and  $\Delta$ CS SARS-CoV-2 virus, concentrated virions by  
109 centrifugation and probed by western blot for spike cleavage (Figure 1D). Like the PV, WT SARS-CoV-  
110 2 harboured both uncleaved and cleaved S2 whereas the virions of the  $\Delta$ CS mutant virus only had  
111 uncleaved spike. Overall, these data confirm that the polybasic CS of SARS-CoV-2 is a *bona fide* furin  
112 CS.

113 The polybasic cleavage site of SARS-CoV-2 spike protein promotes entry into epithelial  
114 cell lines and cultures but adversely affects entry into Vero and 293Ts cells.

115 To investigate whether the S1/S2 furin CS of SARS-CoV-2 plays a role in virus entry, we initially  
116 performed competition assays by taking a mixed population of virus containing 70%  $\Delta$ CS mutant and  
117 30% WT SARS-CoV-2 (as determined by deep sequencing of the S1/S2 CS; Figure 2A) and inoculating  
118 the virus mix onto Vero E6 cells, human intestinal Caco-2 cells or air-liquid interface human airway  
119 epithelial cell cultures (HAEs) at a low multiplicity of infection (MOI) to enable multicycle replication.  
120 We deep sequenced the progeny virus at 72 hours post-inoculation from the Vero E6 or Caco-2  
121 (human intestinal) cells and found that whereas the  $\Delta$ CS mutant outcompeted the WT in Vero E6 cells,  
122 WT became predominant in the Caco-2 cells. In primary HAE cultures, the WT virus also outcompeted  
123 the  $\Delta$ CS virus until the variant was almost undetectable after 72 hours. We also infected Calu-3 (human  
124 lung) cells with either the clonal WT or  $\Delta$ CS viruses at an MOI of 0.1 (Figure 2C). WT virus replicated  
125 robustly and reached peak titres greater than  $10^5$  pfu after 48 hours. Conversely,  $\Delta$ CS virus, appeared  
126 unable to productively infect Calu-3 cells and no infectious titre was detected in supernatant at any  
127 time point.

128 Next, we probed the ability of PV with different mutant spike proteins to enter several  
129 different human cell lines: 293T cells expressing human ACE2, Caco-2 cells or Calu-3 cells (Figure 2D-  
130 F). PV bearing the envelope of amphotropic murine leukaemia virus (MLV-A) or Indiana vesicular

131 stomatitis virus glycoprotein (VSV-G) were used as positive controls for cell entry while PV produced  
132 without any viral glycoproteins (bald) were used as negative controls throughout. As seen in the Vero  
133 E6 cells (Figure 2A), a clear negative correlation was seen between efficiency of furin cleavage of the  
134 spike and entry in the 293T-ACE2 cells (Figure 2D). PV with WT SARS-CoV-2 spike entered 293T-ACE2s  
135 more poorly than SARS-CoV, while mutants without furin cleavage (monoCS, ΔCS, Δflank) entered cells  
136 significantly more efficiently (over 3-fold compared to WT). Introduction of the optimal furin CS (H5CS)  
137 resulted in significantly poorer entry than WT (~10-fold lower;  $P < 0.001$ ). When Caco-2 and Calu-3  
138 cells were tested for PV entry, however, the opposite trend was observed reflecting the efficiency of  
139 virus replication in Caco-2, Calu-3 and primary HAE cells (Figure 2E,F). WT and H5CS spike PV entered  
140 cells efficiently while the mutants unable to be cleaved by furin, including ΔCS, entered cells  
141 significantly less efficiently (>2-fold lower in Caco-2 cells and ~5-fold lower in Calu-3 cells).

142 We next tested the PV which had been generated in the presence of a furin inhibitor for their  
143 ability to enter 293T-ACE2 and Caco-2 cells (Figure 2G,H). In 293T-ACE2, entry of PV bearing WT SARS-  
144 CoV-2 or H5CS spike was boosted 2- to 3-fold if furin was inhibited when the PV was produced (Figure  
145 2G). Conversely, WT SARS-CoV-2 PVs entered Caco-2 cells more poorly (2-fold lower) after inhibition  
146 of furin cleavage, while no effect was seen on the H5CS mutant, potentially due to the majority of  
147 spike still remaining cleaved even after furin inhibition (Figure 1H). No significant differences in entry  
148 were observed for the other mutants or SARS-CoV.

149 Overall, these results suggest that during replication of SARS-CoV-2 in Vero and 293T-ACE2  
150 cells, there is a fitness cost in having a cleaved spike prior to entry, while in primary airway cells and  
151 lung and intestinal cell lines, possessing a processed SARS-CoV-2 furin CS provides an advantage by  
152 facilitating entry.

153 Entry of SARS-CoV-2 into 293T cells is dependent on cathepsins while entry into Caco-  
154 2, Calu-3 and primary HAE cells is dependent on TMPRSS2

155 As well as processing at the S1/S2 CS, coronavirus spike protein requires cleavage at the S2'  
156 site to enable the virus membrane to fuse with the membrane of the host cell. To investigate whether  
157 the different cell entry phenotypes seen in 293T-ACE2/Vero vs Caco-2/Calu-3/HAE cells was due to  
158 differences in the protease use in different cell types, we performed PV entry assays in the presence  
159 of different protease inhibitors: camostat which inhibits serine proteases such as TMPRSS2, and E-  
160 64d, which inhibits cathepsins. Both drugs have previously been shown to be inhibitory to SARS-CoV  
161 and SARS-CoV-2 entry (Hoffmann, Kleine-Weber, Schroeder, et al., 2020; X. Ou et al., 2020).

162 In 293T-ACE2 cells, camostat pre-treatment did not inhibit PV entry whereas E-64d strongly  
163 inhibited entry of SARS-CoV spike PVs, as well as SARS-CoV-2 WT PVs and all CS mutants (Figure 3A).  
164 In Caco-2 cells, a different pattern was seen: camostat had a significant impact on PVs bearing spike  
165 proteins with furin CSs whereas E-64d had a significant impact on PV which were not cleaved by furin  
166 (Figure 3B). In Calu-3 cells, camostat significantly inhibited entry of all coronavirus PVs while E-64d  
167 also had a modest, but significant ( $P < 0.05$ ), effect on the  $\Delta$ CS mutant (Figure 3C). Control PV  
168 expressing MLV-A or VSV-G, which are not reliant on cathepsins or serine proteases for entry  
169 (Hoffmann, Kleine-Weber, Schroeder, et al., 2020), were not significantly affected by either drug in  
170 any cell line.

171 To confirm that dependence of serine proteases for entry, as observed in Caco-2 and Calu-3  
172 cells, was seen with whole SARS-CoV-2 virus in primary airway cells, we examined multicycle  
173 replication of clonal WT and  $\Delta$ CS viruses on HAE cells in the presence or absence of camostat (Figure  
174 3D). Our previous results showed that the  $\Delta$ CS virus was selected against on HAE cells and, indeed,  
175 the  $\Delta$ CS virus grew to significantly lower titres than WT. Addition of 50  $\mu$ M camostat almost  
176 completely abrogated virus replication of both  $\Delta$ CS and WT virus (Figure 3D), showing that in HAEs,  
177 efficient cleavage by serine proteases facilitates efficient entry.

178 To investigate whether differences in endogenous levels of different proteases could explain  
179 the phenotypic differences seen in the different human cell lines, as well as HAEs, we quantified the  
180 expression of several different proteases using qPCR (Figure 3E-H). All three human cell lines and the  
181 primary HAE cultures expressed ACE2 and cathepsin L to varying degrees. However, 293T-ACE2 cells  
182 lacked any detectable TMPRSS2 expression, likely explaining why camostat had little effect on PV entry  
183 into these cells. Although not tested here, several previous studies have shown Vero E6 cells also  
184 express no endogenous TMPRSS2 (Bertram et al., 2010; Shirato et al., 2013).

185 Expression of TMPRSS2 promotes entry of SARS-CoV-2 expressing a full polybasic  
186 cleavage site.

187 To investigate whether expression of TMPRSS2 was responsible for the advantage seen by  
188 viruses with furin cleavable spike proteins in Caco-2 and Calu-3 cells, we transiently co-expressed ACE2  
189 with or without TMPRSS2 in 293T cells and compared the entry of furin cleaved and non-furin cleaved  
190 PV (Figure 4A). We found that entry of all coronavirus PVs was promoted by the expression of  
191 TMPRSS2, even though TMPRSS2 expression led to lower levels of cell associated ACE2 due to ACE2  
192 being a substrate of TMPRSS2 (Supplementary Figure S1A) (Shulla et al., 2011). The TMPRSS2  
193 enhancement of PV entry was particularly potent for the PVs harbouring furin CS containing spike  
194 (>15-fold), compared to the non furin-cleaved mutants (<10-fold) indicating that expression of  
195 TMPRSS2 favours the entry into cells of PVs with furin CSs.

196 The furin cleavage site of SARS-CoV-2 allows escape from IFITM2/3 proteins in TMPRSS2  
197 expressing cells

198 The enhanced replication shown by SARS-CoV-2 with furin pre-cleaved spike to utilise  
199 TMPRSS2 to enter cells efficiently suggested this virus may prefer to enter cells via membranes near  
200 the cell surface or in the early endosome rather than be trafficked into late endosomes where it could  
201 be cleaved by host cathepsins. We hypothesised that the wild type virus may be avoiding host  
202 restriction factors in the endosome, such as IFITM2/3 proteins, which have previously been shown to

203 be able to restrict SARS-CoV and SARS-CoV-2 entry (Huang et al., 2011; Zhao et al., 2020; Zheng et al.,  
204 2020). The antifungal agent amphotericin B (amphoB) has been well described as inhibiting the  
205 restriction imposed by IFITM proteins, particularly the endosomal/lysosomal localised IFITM2/3,  
206 potentially modulating the host membrane fluidity required for efficient restriction (Lin et al., 2013;  
207 Zhao et al., 2020; Zheng et al., 2020). We could also show that 293T-ACE2, Caco-2, Calu-3 and HAEs all  
208 constitutively expressed IFITM3, even in the absence of exogenous interferon (Figure 3E-H). We  
209 treated cells with amphoB and investigated the effect on PV entry. In 293T-ACE2 cells, entry of all  
210 coronavirus PV was improved by amphoB pre-treatment, with the largest effect exerted upon PVs  
211 with polybasic CS containing spikes (Figure 4B). Conversely, in Caco-2 and Calu-3 cells, the opposite  
212 effect was seen – entry of PVs with non-furin CS spikes was boosted, in some cases significantly by  
213 amphoB treatment, whereas there was little or no effect on the entry of PVs with furin CS containing  
214 spikes (Figure 4C,D).

215 Next, we took 293T cells and transiently co-transfected a combination of ACE2 and TMPRSS2  
216 in the presence or absence of IFITM3. Entry of PVs with furin CS containing spikes were less inhibited  
217 by IFITM3 than those with spikes that could not be furin cleaved (Figure 4E, Supplementary Figure  
218 S1B).

219 Finally, we investigated the effect of amphoB treatment on SARS-CoV-2 replication in primary  
220 airway cells. AmphoB had no effect on WT virus replication, but greatly increased the replication of  
221 the ΔCS mutant (Figure 4F). This implies that IFITM proteins, such as IFITM3, are a major block for  
222 entry of viruses without furin CSs in these cells.

223 The SARS-CoV-2 polybasic cleavage site promotes replication in the respiratory tract  
224 and transmission in a ferret model

225 To investigate whether the furin CS plays a role in the transmission of SARS-CoV-2, we used  
226 ferrets as an in vivo model. Ferrets are commonly used in transmission studies of respiratory  
227 pathogens such as influenza and, more recently, SARS-CoV-2 (Belser et al., 2018; Kim et al., 2020;

228 Richard et al., 2020). Four ferrets per group were each infected intranasally with  $10^5$  pfu of clonally  
229 purified stocks of the WT or  $\Delta$ CS mutant SARS-CoV-2 viruses. After 24 hours, naïve contact ferrets  
230 were placed into each cage. All ferrets were nasal washed daily for the following 2 weeks and virus  
231 shedding in the nose was titrated by qRT-PCR and by TCID<sub>50</sub> (Figure 5A,B, Supplementary Figure S2A,B).  
232 All eight directly inoculated ferrets shed virus robustly for 9-12 days (Figure 5A). The WT infected  
233 group shed more virus in the nose than ferrets infected with  $\Delta$ CS virus, indicated by higher infectivity  
234 and higher E gene copy numbers, the latter significant at days 2-4. In the WT group, 2/4 contact ferrets  
235 became productively infected indicated by infectious virus, E gene loads in nasal wash, and  
236 seroconversion, whereas no transmission from donor ferret infected with  $\Delta$ CS mutant virus was  
237 detected (Figure 5B, Supplementary Figures S2A-C). In nasal washes of the two remaining ferrets  
238 exposed to donors infected with WT virus, low E gene copy numbers were detected but no infectious  
239 virus was measured by TCID<sub>50</sub>, and these animals remained seronegative at 14 days post exposure,  
240 implying these ferrets were genuinely not infected in contrast to all directly infected animals and the  
241 two virus positive WT infected sentinels (Supplementary Figure S2C).

242 Next, a competition assay was performed whereby four ferrets were inoculated intra-nasally  
243 with  $10^5$  pfu of the previously described mixture of WT and  $\Delta$ CS virus at a 30:70 ratio, as determined  
244 by deep sequencing. One day post-inoculation, naïve contact ferrets were cohoused with each directly  
245 inoculated animal and all animals were nasal washed daily. All directly inoculated ferrets became  
246 productively infected, shedding infectious virus and detectable E gene in nasal wash for between 9-  
247 12 days (Figure 5C). Interestingly, which virus genotype became dominant in the nasal washes of the  
248 directly infected ferrets appeared to vary stochastically; in two animals the WT virus became  
249 predominant by day 2, and levels of infectious virus and E gene detected in their nasal wash was  
250 highest. In the nasal wash of the other two directly inoculated animals, the  $\Delta$ CS virus remained the  
251 majority species or outcompeted the WT over the course of the experiment. Productive transmission  
252 was only recorded in a single contact and interestingly, this animal was co-caged with one of the  
253 animals that was shedding predominantly WT virus. The  $\Delta$ CS genotype was detectable in this single

254 contact at low levels on day 3, 8 and 9, but at all times the WT genotype was clearly predominant.  
255 Furthermore, this was the only contact ferret to seroconvert, confirming the other 3 contact ferrets  
256 were not productively infected (Supplementary Figure S3D). No ferrets in either group showed  
257 appreciable fever or weight loss (Supplementary Figures S3A-C, S2D,E). Together these results suggest  
258 that the furin CS of SARS-CoV-2 is a determinant of transmission in the ferret model.  
  
259 SARS-CoV-2 spike variants with deletions or mutations in the polybasic cleavage site are  
260 detectable in human tissues.

261 Finally, we wanted to investigate whether spike deletion mutants could be found in human  
262 clinical samples and, if so, whether they were more likely to be found in a particular organ. Initially we  
263 downloaded 100,000 genome sequences from GISAID and found 2 sequences from nasal swabs with  
264 CS deletions (Supplementary Table S1). Next, we sequenced the S1/S2 CS from 24 previously described  
265 post-mortem samples taken from five different post-mortems and including tissues from the  
266 respiratory and gastrointestinal tract, the brain, heart, bone marrow, kidney, tongue and spleen  
267 (Hanley et al., 2020). Sequencing revealed very low levels of viral RNA bearing different S1/S2 CS  
268 deletion (<1%) from heart and spleen tissue from separate patients (Supplementary Table S2). The  
269 three separate deletions reported in Supplementary Table S1 have not previously been reported but  
270 are similar to those seen upon passage in Vero E6 cells. OS5 deletes 4 amino acids after the CS similar  
271 to a deletion reported in a recent preprint (Sasaki et al., 2020); OS19-1 overlaps with most of ΔFlank  
272 and OS19-2 completely removes the S1/S2 site, similar to ΔCS. We have also observed identical  
273 deletions to OS19-2 upon passaging the clonal WT virus in Vero E6 cells. These results are consistent  
274 with the conclusion that S1/S2 cleavage site deletions can arise naturally in vivo, albeit at a very low  
275 rate.

## 276 Discussion

277 An insertion of 4 amino acids in the SARS-CoV-2 spike protein created a suboptimal furin  
278 cleavage site (CS). Here, we propose a mechanism by which this conferred an advantage to the virus  
279 in the human airway and enabled efficient human-to-human transmission. We show that pre-cleavage  
280 of the spike during viral egress enhanced entry of progeny virions into TMPRSS2-expressing cells such  
281 as those abundant in respiratory tissue. TMPRSS2 cleaves spike at S2' and facilitates entry at the cell  
282 surface (or possibly the early endosome) as opposed to entry through the endosome. This allows virus  
283 to avoid the otherwise potent IFITM restriction factors that reside in the late endosome and lysosome  
284 and inhibit viral membrane fusion in these compartments. Viruses that lack a polybasic S1/S2 CS  
285 cannot be cleaved by furin in producer cells and are thus forced to enter the next cell they infect  
286 through the endosome where the spike can be cleaved at S1/S2 and S2' by cathepsins. However, pre-  
287 cleaved spike is not always advantageous: in cell types lacking TMPRSS2 expression, such as Vero E6,  
288 viruses without the furin CS gain an advantage, potentially because they are more stable, since spike  
289 cleavage may result in premature loss of the S1 subunit altogether and abrogate receptor binding. Our  
290 results show that, in contrast with WT SARS-CoV-2, a virus with a deleted furin CS did not replicate to  
291 high titres in the upper respiratory tract of ferrets and did not transmit to cohoused sentinel animals,  
292 in agreement with recent results from similar experiments with hamsters (Y. Zhu et al., 2020). It is not  
293 yet clear whether transmission is blocked due to the lower titres released from the directly inoculated  
294 donor ferrets, or to a lower ability to initiate infection in the TMPRSS2-rich cells of the nasal epithelium  
295 or a combination of these. We have found that furin CS deletions arise naturally in various different  
296 human organs during severe infection, but rarely and at low levels. Indeed, we note only 2 recorded  
297 genomes on GISAID out of 100,690 (as of 16/9/20) with furin CS deletions (Supplemental Table S1).  
298 Given the ease of loss of the furin CS in cell culture, the lack of these mutants in sequenced isolates is  
299 further evidence that the furin CS is essential for sustained transmission of SARS-CoV-2 in humans.

300                   Presence of a furin CS at the S1/S2 junction is not uncommon in human coronaviruses; two of  
301                   the four seasonal coronaviruses that transmit efficiently in humans, hCoV-HKU1 and hCoV-OC43, both  
302                   contain furin CSs while MERS-CoV contains a suboptimal dibasic furin CS (Le Coupanec et al., 2015;  
303                   Millet & Whittaker, 2014). However, the other two human seasonal coronaviruses, hCoV-229E and  
304                   the ACE2 binding hCoV-NL63, do not contain furin CSs in their spike proteins seemingly without any  
305                   detriment to transmissibility. Thus, furin-mediated cleavage of spike is not an absolute requirement  
306                   for efficient human respiratory transmission. Furthermore, the original 2003 SARS-CoV lacked a furin  
307                   CS and was clearly transmitted between people, although this usually occurred during a symptomatic  
308                   phase rather than asymptotically or pre-symptomatically, thus allowing the virus outbreak to be  
309                   controlled by public health measures (Liu, Gayle, Wilder-Smith, & Rocklov, 2020). Several recent  
310                   studies have investigated the pathogenicity of naturally occurring or engineered deletion mutants in  
311                   the hamster model, and shown that viruses lacking the furin CS are attenuated for replication and  
312                   pathogenicity (Johnson et al., 2020; Lau et al., 2020; Wang et al., 2020; Wong et al., 2020). We, like  
313                   others, did not find that SARS-CoV-2 induced significant clinical signs in ferrets, so were unable to  
314                   assess the effect of the CS mutation on viral pathogenesis here. Nonetheless, we did observe  
315                   transmission between ferrets suggesting clinical signs are not required for transmission. A further  
316                   single study also found a CS deletion mutant virus did not transmit between hamsters (Y. Zhu et al.,  
317                   2020). Two studies suggest that the furin cleavage peptide motifs at the S1/S2 CS enables WT SARS-  
318                   CoV-2 virus to utilise neuropilin as a cellular attachment/entry factor (Cantuti-Castelvetro et al., 2020;  
319                   Daly et al., 2020). However, since 293T cells express neuropilin and lentiviral pseudotypes (PV) lacking  
320                   the furin CS enter these cells more efficiently than PV containing it, this suggests that neuropilin is not  
321                   responsible for the entry differences between furin cleavage mutants.

322                   IFITM proteins are well characterised restriction factors of many enveloped viruses. Human  
323                   IFITM3, for example, is a potent inhibitor of influenza infection and naturally occurring variants have  
324                   been associated with severe influenza infection (Everitt et al., 2012; Huang et al., 2011; Zhang et al.,  
325                   2013). IFITM proteins have also been shown to inhibit coronavirus entry (Huang et al., 2011; Wrensch,

326 Winkler, & Pohlmann, 2014), although hCoV-OC43 and hCoV-HKU1 are unique in that IFITM proteins  
327 appear to act as entry factors to these viruses (Zhao et al., 2014; Zhao et al., 2018). There is growing  
328 evidence that IFITM proteins inhibit SARS-CoV-2 syncytia formation or pseudoviral or viral entry  
329 (Bozzo et al., 2020; Buchrieser et al., 2020; Shi et al., 2020), as we confirm here. This may partly explain  
330 the vulnerability of SARS-CoV-2 to IFN treatment (Mantlo, Bukreyeva, Maruyama, Paessler, & Huang,  
331 2020). A recent preprint has suggested that under certain conditions IFITM proteins can have a modest  
332 pro-viral effect on SARS-CoV-2 virus growth (Bozzo et al., 2020). This is not inconsistent with our data  
333 which showed that amphotericin B mediated inhibition of IFITM proteins had no effect on, and if  
334 anything, slightly inhibited, WT SARS-CoV-2 virus replication in primary human cells.

335 Our study confirms TMPRSS2 as a potential drug target. Whilst inhibition of TMPRSS2  
336 protease activity would not prevent infection via the endosome, using this pathway is detrimental to  
337 virus replication in airway cells. We have shown in this study that the protease inhibitor, camostat, is  
338 highly efficient at blocking SARS-CoV-2 replication in human airway cells and we note that clinical trials  
339 are ongoing [ClinicalTrials.gov Identifier: NCT04455815]. Our study also confirms the limitations of  
340 relying on Vero E6 cells as a system for developing classes of drugs such as entry inhibitors as they do  
341 not accurately reflect the preferred entry mechanism of SARS-CoV-2 into human airway cells  
342 (Hoffmann, Mosbauer, et al., 2020; T. Ou et al., 2020). Indeed the data here explains why chloroquine  
343 is ineffective in clinic against SARS-CoV-2 (Hoffmann, Mosbauer, et al., 2020), since during replication  
344 in the human airway WT SARS-CoV-2 has evolved to enter cells without the need for endosomal  
345 acidification. Monitoring wild coronaviruses will likely be important in predicting and preventing  
346 future pandemics. We suggest that a furin CS in the SARS lineage is a cause for concern. The polybasic  
347 insertion to the S1/S2 CS provides a significant fitness advantage in TMPRSS2 expressing cells and is  
348 likely essential for efficient human transmission.

349                   Materials and Methods

350                   *Biosafety and ethics statement*

351                   All work performed was approved by the local genetic manipulation (GM) safety committee of  
352                   Imperial College London, St. Mary's Campus (centre number GM77), and the Health and Safety  
353                   Executive of the United Kingdom, under reference CBA1.77.20.1. Animal research was carried out  
354                   under a United Kingdom Home Office License, P48DAD9B4.

355                   Human samples used in this research project were obtained from the Imperial College Healthcare  
356                   Tissue Bank (ICHTB). ICHTB is supported by the NIHR Biomedical Research Centre based at Imperial  
357                   College Healthcare NHS Trust and Imperial College London. ICHTB is approved by Wales REC3 to  
358                   release human material for research (17/WA/0161), and the samples for this project (R20012) were  
359                   issued from subcollection reference number MED\_MO\_20\_011.

360                   *Cells and viruses*

361                   African green monkey kidney cells (Vero E6) and human embryonic kidney cells (293T) were  
362                   maintained in Dulbecco's modified Eagle's medium (DMEM), 10% fetal calf serum (FCS), 1% non-  
363                   essential amino acids (NEAA), 1% penicillin-streptomycin (P/S). Human epithelial colorectal  
364                   adenocarcinoma cells (Caco-2) and human lung cancer cells (Calu-3) were maintained in DMEM,  
365                   20% FCS, 1% NEAA, 1% P/S. VeroE6/TMPRSS2 cells were obtained from the Centre for AIDS Reagents  
366                   (National Institute for Biological Standards and Control) (Matsuyama et al., 2020; Nao et al., 2019),  
367                   and maintained in DMEM, 10% FCS, 1% NEAA, 1% P/S, 1 mg/ml Geneticin (G418). Air liquid interface  
368                   Human airway epithelial cells (HAEs) were purchased from Epithelix and maintained in Mucilair cell  
369                   culture medium (Epithelix). All cell lines were maintained at 37°C, 5% CO<sub>2</sub>

370                   293T-hACE2 were generated by transducing 293Ts with an ACE2 expressing lentiviral vector,  
371                   MT126, and selecting with 2 µg/ml puromycin, after selection cells were subsequently maintained  
372                   with 1 µg/ml of puromycin.

373                   The mixed SARS-CoV-2 WT/deletion virus mix was produced as previously described (Davidson  
374                   et al., 2020). Briefly, the mix was generated by passaging the strain England/2/2020 (VE6-T), isolated  
375                   by Public Health England (PHE), in Vero E6 cells whereby the deletion spontaneously arose (Davidson  
376                   et al., 2020). The WT SARS-CoV-2 strain SARS-CoV-2 strain England/2/2020 (VE6-T) and the ΔCS  
377                   mutant present in the original mixed stock were purified by serially diluting the stock (10-fold  
378                   dilutions) in MEM supplemented with 2% FCS and adding the dilutions to either Vero E6 or Caco-2  
379                   cells in a 96 well plate. After 5 days incubation at 37 °C in 5% CO<sub>2</sub>, the culture supernatants in wells  
380                   showing CPE at the highest dilution were again diluted and passaged on the same cells. After a further  
381                   5 days incubation, a 20 µl aliquot of culture supernatant from wells showing CPE at the highest dilution  
382                   were used for RNA extraction and RT-PCR using a primer set designed to discriminate the WT and ΔCS  
383                   mutant viruses. Culture supernatants containing either the WT or ΔCS mutant virus, with no sign of a  
384                   mixed virus population were used to produce large scale stocks in Vero E6 cells. The presence of the  
385                   expected virus in the stocks was verified by direct RNA sequencing using an Oxford Nanopore flow cell  
386                   as previously described (Davidson et al., 2020). Clonally pure viruses were then further amplified by  
387                   one additional passage in Vero E6/TMPRSS2 cells to make the working stocks of the viruses used  
388                   throughout this study.

389                   For plaque assays Vero E6 cells were used at 70-80% confluence. Cells were washed with PBS  
390                   then serial dilutions of inoculum, diluted in serum-free DMEM, 1% NEAA, 1% P/S, were overlayed onto  
391                   cells for one hour at 37°C. Inoculum was then removed and replaced with SARS-CoV-2 overlay media  
392                   (1x minimal essential media [MEM], 0.2% w/v bovine serum albumin, 0.16% w/v NaHCO<sub>3</sub>, 10mM  
393                   Hepes, 2mM L-Glutamine, 1x P/S, 0.6% w/v agarose). Plates were incubated for 3 days at 37°C before  
394                   overlay was removed and cells were stained for 1 hour at RT in crystal violet solution.

395                   To titrate virus by TCID<sub>50</sub> Vero E6 cells were used at 70-80% confluence. Serial dilutions of  
396                   virus, diluted in serum-free DMEM, 1% NEAA, 1% P/S, were added to each well and cells were left for  
397                   5 days before they were fixed with 2x crystal violet solution and analysed. 4 replicates of each sample

398 were performed in tandem. TCID<sub>50</sub> titres were determined by the Spearman-Kärber method (Kärber,  
399 1931).

400 *Plasmids and cloning*

401 Lentiviral packaging constructs pCSLW and pCAGGs-GAGPOL were made as previously  
402 described (Long, Wright, Molesti, Temperton, & Barclay, 2015). The codon-optimised spike proteins  
403 of SARS-CoV-2, SARS-CoV and MERS-CoV were a kind gift from Professor Robin Shattock, Imperial  
404 College London (McKay et al., 2020). Mutant SARS-CoV-2 expression plasmids were generated by site-  
405 directed mutagenesis. The lentiviral expression vector for human ACE2, MT126, was a kind gift from  
406 Caroline Goujon, University of Montpellier. ACE was further cloned into pCAGGs with the addition of  
407 a C-terminal FLAG-tag. TMPRSS2 expression plasmid was a kind gift from Roger Reeves (Addgene  
408 plasmid #53887 ; <http://n2t.net/addgene:53887> ; RRID:Addgene\_53887, (Edie et al., 2018)).

409 *Syncytia formation assay*

410 Vero E6 cells were seeded in 96-well plates (6.5x10<sup>3</sup> cells per well) to reach 70-80% confluence  
411 on the subsequent day. Transfection was performed using 100 ng of expression plasmid using 0.3 µl  
412 of FuGENE HD Transfection Reagent (Promega E2311) in 20 µl of Opti-MEM medium (Life  
413 Technologies). At 48 hr after drug treatment, plates were washed in 100 µL/well of 1xPBS and fixed in  
414 40 µl 4% PFA for 10 min at RT. After fixation cells were permeabilized in 0.1% Tritonx100 for 10 min  
415 at RT. Nuclei were stained using Hoechst 33342 (H3570 ThermoFisher), according to the  
416 manufacturer's instructions.

417 Image acquisition was performed using the Operetta CLS high content screening microscope  
418 (Perkin Elmer) with a Zeiss 20x (NA=0.80) objective. A total of 25 fields per well were imaged for the  
419 Hoechst 33342 channel (Excitation (Ex) 365-385nm, Emission (Em) 430-500nm). Images were  
420 subsequently analysed, using the Harmony software (PerkinElmer). Images were first flatfield-  
421 corrected and nuclei were segmented using the “Find Nuclei” analysis module (Harmony). The  
422 thresholds for image segmentation were adjusted according to the signal-to-background ratio.

423 Splitting coefficient was set in order to avoid splitting of overlapping nuclei (fused cells). All the cells  
424 that had a nuclear area greater than 3 times the average area of a single nucleus were considered as  
425 fused. Data were expressed as a percentage of fused cells by calculating the average number of fused  
426 cells normalized on the total number of cells per well.

427 *Lentiviral pseudotype assays*

428 Lentiviral pseudotypes (PV) were generated as previously described (Long et al., 2015; Sumner  
429 et al., 2020). Briefly, 10cm<sup>2</sup> dishes of 293T cells were co-transfected with a mixture of 1 µg of the HIV  
430 packaging plasmid pCAGGs-GAGPOL, 1.5 µg of the luciferase reporter construct, pCSLW and 1 µg of  
431 each envelope protein in pcDNA3.1. PV containing supernatants were harvested at 48- and 72-hours  
432 post-transfection, passed through a 0.45 µm filter, aliquoted and frozen at -80°C. When used, the pro-  
433 protein convertase inhibitor Decanoyl-RVKR-CMK (Calbiochem) was applied to cells at a concentration  
434 of 5 µM, 3 hours post-transfection. Concentrated PV were produced by ultracentrifugation at 100,000  
435 x g for 2 hours over a 20% sucrose cushion.

436 Cells were transduced by PV for 48 hours before lysis with cell culture lysis buffer (Promega).  
437 Luciferase luminescence was read on a FLUOstar Omega plate reader (BMF Labtech) using the  
438 Luciferase Assay System (Promega). The cathepsin inhibitor E-64d (Sigma-Aldrich), the serine protease  
439 inhibitor camostat mesylate (Abcam), or the antifungal and IFITM3 inhibitor Amphotericin B (Sigma-  
440 Aldrich) was pre-applied to cells for 1 hour at a concentration of 50 µM before addition of PV.

441 *Deep sequencing using primer ID*

442 RNA was extracted from ferret nasal washes or cell supernatants using the QIAamp Viral RNA  
443 Mini Kit (Qiagen) with carrier RNA. RNA was reverse transcribed using Superscript IV (Invitrogen) and  
444 a barcoded primer for Primer ID  
445 (TGC GTT GAT ACC ACT GCT TNNNNNNNNNNNACTGAATTTCTGCACCAAG). Primer ID attaches a  
446 unique barcode to each cDNA molecule during reverse transcription and allows for PCR and  
447 sequencing error correction (Goldhill et al., 2019; Goldhill et al., 2018; Jabara, Jones, Roach, Anderson,  
448 & Swanstrom, 2011). PCR was performed using KOD polymerase (Merck) and the following primers  
449 (CAACTTACTCCTACTTGGCGT and XXXXTGCGTTGATACCACTGCTTT) giving a 272bp amplicon. XXXX was  
450 a 4-base barcode (CACA, GTTG, AGGA or TCTC) to allow for additional multiplexing. Samples were  
451 pooled and prepared for sequencing using NebNext Ultra II (NEB), then sequenced on an Illumina  
452 MiSeq with 300bp paired-end reads. Sequences were analysed in Geneious (v11) and a pipeline in R.  
453 Forward and reverse reads were paired using FLASH (<https://ccb.jhu.edu/software/FLASH>) before  
454 being mapped to a reference sequence and consensus sequences made for each barcode. A minimum  
455 cut-off of 3 reads per barcode was chosen. Raw sequences were deposited at [www.ebi.ac.uk/ena](http://www.ebi.ac.uk/ena),  
456 project number PRJEB40394. The analysis pipeline can be found at [github.com/Flu1/Corona](https://github.com/Flu1/Corona)

457 *Deep sequencing from post-mortem samples*

458 RNA from human post-mortem tissues from SARS-CoV-2 patients where COVID-19 was listed  
459 clinically as the cause of death were sourced and processed as previously described (Hanley et al.,  
460 2020). Briefly, fresh tissue was processed within biosafety level 3 facilities and total RNA was extracted  
461 using TRIzol (Invitrogen)-chloroform extraction followed by precipitation and purification using an  
462 RNeasy mini kit (Qiagen). RNA was reverse transcribed using Superscript IV (Invitrogen) and the  
463 following primer (GTCTTGGTCATAGACACTGGTAG). PCR was performed using KOD polymerase  
464 (Merck) and the following primers (GTCTTGGTCATAGACACTGGTAG and  
465 GGCTGTTAATAGGGGCTGAAC) giving a 260bp amplicon. Samples were prepared for sequencing using

466 NebNext Ultra II (NEB), then sequenced on an Illumina MiSeq with 300bp paired-end reads. Sequences  
467 were analysed in Geneious (v11) and a pipeline in R. Forward and reverse reads were paired using  
468 FLASh (<https://ccb.jhu.edu/software/FLASH>) before being mapped to a reference sequence. Raw  
469 sequences were deposited at [www.ebi.ac.uk/ena](http://www.ebi.ac.uk/ena), project number PRJEB40394. The analysis pipeline  
470 can be found at [github.com/Flu1/Corona](https://github.com/Flu1/Corona).

471 *Human Clinical Samples*

472 A total of 100,690 SARS-CoV-2 genomes were downloaded from GISAID on 16/9/2020 and  
473 aligned to 234bp from the spike protein using Geneious. In frame deletions were identified in R and  
474 analysed to ensure that samples had not been passaged prior to sequencing. Code for this analysis  
475 can be found at [github.com/Flu1/Corona](https://github.com/Flu1/Corona).

476 *Ferret transmission studies*

477 Ferret transmission studies were performed in a containment level 3 laboratory, using a  
478 bespoke isolator system (Bell Isolation Systems, U.K). Outbred female ferrets (16-20 weeks old),  
479 weighing 750-1000 g were used.

480 Prior to the study, ferrets were confirmed to be seronegative against SARS-CoV-2. Four donor  
481 ferrets were inoculated intranasally with 200  $\mu$ l of  $10^5$  pfu of virus mix while lightly anaesthetised with  
482 ketamine (22 mg/kg) and xylazine (0.9 mg/kg). To assess direct contact transmission one naïve direct  
483 contact ferrets were introduced into each cage 1-day post initial inoculation.

484 All animals were nasal washed daily, while conscious, by instilling 2 mL of PBS into the nostrils,  
485 the expectorate was collected into disposable 250 ml sample pots. Ferrets were weighed daily post-  
486 infection, and body temperature was measured daily via subcutaneous iPTT-300 transponder (Plexx  
487 B.V, Netherlands).

488 *Virus Neutralisation assay*

489 The ability of ferret sera to neutralise wild type SARS-CoV-2 virus was assessed by  
490 neutralisation assay on Vero E6 cells. Heat-inactivated sera were serially diluted in assay diluent  
491 consisting of DMEM (Gibco, Thermo Fisher Scientific) with 1% penicillin-streptomycin (Thermo Fisher  
492 Scientific), 0.3% BSA fraction V (Thermo Fisher Scientific). Serum dilutions were incubated with 100  
493 TCID<sub>50</sub>/well of virus in assay diluent for 1 h at RT and transferred to 96-well plates pre-seeded with  
494 Vero E6 cells. Serum dilutions were performed in duplicate. Plates were incubated at 37°C, 5% CO<sub>2</sub>  
495 for 5 days before adding an equal volume of 2X crystal violet stain to wells for 1 h. Plates were washed,  
496 wells were scored for cytopathic effect and a neutralisation titre calculated as the reciprocal of the  
497 highest serum dilution at which full virus neutralisation occurred.

498 *qPCR*

499 Viral RNA was extracted from Ferret nasal washes using the Qiagen Viral RNA mini kit,  
500 according to manufacturer's instructions.

501 Quantitative real-time RT-PCR (qRT-PCR) was performed using 7500 Real Time PCR system  
502 (ABI) in 20 µl reactions using AgPath-ID One-Step RT-PCR Reagents 10 µl RT-PCR buffer (2X) (Thermo  
503 Fisher), 5µl of RNA, 1 µl forward (5' ACAGGTACGTTAATAGTTAATAGCGT 3') and reverse primers (5'  
504 ATATTGCAGCAGTACGCACACA 3') and 0.5 µl probe (5' FAM-ACACTAGCCATCCTACTGCGCTTCG -BBQ  
505 3'). The following conditions were used: 45°C for 10 min, 1 cycle; 95°C for 15 min, 1 cycle; 95°C for 15  
506 sec then 58°C for 30 sec, 45 cycles. For each sample, the C<sub>t</sub> value for the target E gene was determined.  
507 Based on the standard curves, absolute E gene copy numbers were calculated.

508 RNA was extracted from cells using RNA extraction kits (QIAGEN, RNeasy Mini Kit, cat. 74106)  
509 following the manufacturer's instructions. Complementary DNA (cDNA) was synthesized in a reverse  
510 transcription step using Oligo-dT (RevertAid First Strand cDNA Synthesis, ThermoScientific, cat:  
511 K1621). To quantify mRNA levels, real-time quantitative PCR analysis with a gene specific primer pair

512 using SYBR green PCR mix (Applied Biosystems, cat: 4385612) was performed and data was analysed  
513 on the Applied Biosystems ViiATM 7 Real-Time PCR System. The following primers were used:

primer	sequence	reference
ACE2-Fwd	AAACATACTGTGACCCCGCAT	(Ma et al., 2020)
ACE2-Rev	CCAAGCCTCAGCATATTGAAC A	(Ma et al., 2020)
TMPRSS2-Fwd	ACTCTGGAAGTTCATGGCAG	(Ma et al., 2020)
TMPRSS2-Rev	TGAAGTTGGTCCGTAGAGGC	(Ma et al., 2020)
CTSL-Fwd	GCATGGGTGGCTACGTAAAG	(Xu et al., 2016)
CTSL-Rev	TCCCCAGTCAAGTCCTTCCT	(Xu et al., 2016)
FURIN-Fwd	CTACACAGGGCACGGCATTG	(Z. Zhou et al., 2014)
FURIN-Rev	CCACACCTACACCACAGACAC	(Z. Zhou et al., 2014)
IFITM3-Fwd	GGTCTCGCTGGACACCAT	(Xu-yang et al., 2017)
IFITM3-Rev	TGTCCCTAGACTTCACGGAGT A	(Xu-yang et al., 2017)
β-actin-Fwd	GTACGCCAACACAGTGCTG	(H. Li et al., 2018)
β-actin-Rev	CGTCATACTCCTGCTTGCTG	(H. Li et al., 2018)

514 The gene expression was calculated by normalizing target gene expression to  $\beta$  -actin for each sample  
515 and expressed as  $2 \Delta Ct$ .

516

517 *Western Blotting*

518 To investigate cleavage of spike protein 293T cells transfected with 2.5  $\mu$ g of spike expression  
519 plasmids (or empty vector). After 48 hours cells were lysed in RIPA buffer (150mM NaCl, 1% NP-40,  
520 0.5% sodium deoxycholate, 0.1% SDS, 50mM TRIS, pH 7.4) supplemented with an EDTA-free protease

521 inhibitor cocktail tablet (Roche). Cell lysates were then mixed with 4x Laemmli sample buffer (Bio-Rad)  
522 with 10% β-mercaptoethanol. Concentrated PV as described above were also diluted in Laemmli  
523 buffer.

524 Membranes were probed with mouse anti-FLAG (F1804, Sigma), mouse anti-tubulin (abcam;  
525 ab7291), mouse anti-p24 (abcam; ab9071), rabbit anti-TMPRSS2 (abcam; ab92323), rabbit anti-  
526 Fragilis/IFITM3 (abcam; ab109429), rabbit anti-SARS spike protein (NOVUS; NB100-56578) or rabbit  
527 anti-SARS-CoV-2 nucleocapsid (SinoBiological; 40143-R019). Near infra-red (NIR) secondary  
528 antibodies, IRDye® 680RD Goat anti-mouse (abcam; ab216776), IRDye® 680RD Goat anti-rabbit  
529 (abcam; ab216777), IRDye® 800CW Goat anti-mouse (abcam; ab216772), or IRDye® 800CW Goat anti-  
530 rabbit (abcam; ab216773)) were subsequently used. Western blots were visualised using an Odyssey  
531 Imaging System (LI-COR Biosciences).

## 532 Acknowledgments

533 SARS-CoV-2 virus was initially provided by Public Health England and we would like to thank Maria  
534 Zambon, Robin Gopal and Monika Patel for their help. This work was supported by BBSRC grants  
535 BB/R013071/1 (TPP, WB); BB/R007292/1 (LB, WB); BB/S008292/1 (JB, WB); BB/M02542X/1 (ADD,  
536 DAM) and Wellcome Trust grants 205100 (DHG, RYSD, WB); 200187 (JZ, RF, WB). This work was also  
537 supported by MRC grant MR/R020566/1 (MKW, ADD) and US FDA grant HHSF223201510104C (ADD,  
538 DAM). Additional support was provided from a grant from the King's College London King's Together  
539 Programme and the King's College London BHF Centre of Research Excellence grant RE/18/2/34213  
540 to MG. OCS was supported by a Wellcome Trust studentship, RK was supported by Wellcome  
541 fellowship 216353/Z/19/Z, RP was supported by an MRC DTP studentship, JAH was supported by a  
542 BBSRC DTP studentship and ES was supported by an Imperial College President's Scholarship.

543

## 544 References

545 Andersen, K. G., Rambaut, A., Lipkin, W. I., Holmes, E. C., & Garry, R. F. (2020). The proximal origin of  
546 SARS-CoV-2. *Nat Med*, 26(4), 450-452. doi:10.1038/s41591-020-0820-9

547 Belouzard, S., Chu, V. C., & Whittaker, G. R. (2009). Activation of the SARS coronavirus spike protein  
548 via sequential proteolytic cleavage at two distinct sites. *Proc Natl Acad Sci U S A*, 106(14),  
549 5871-5876. doi:10.1073/pnas.0809524106

550 Belser, J. A., Barclay, W., Barr, I., Fouchier, R. A. M., Matsuyama, R., Nishiura, H., . . . Yen, H. L. (2018).  
551 Ferrets as Models for Influenza Virus Transmission Studies and Pandemic Risk Assessments.  
552 *Emerg Infect Dis*, 24(6), 965-971. doi:10.3201/eid2406.172114

553 Bertram, S., Glowacka, I., Blazejewska, P., Soilleux, E., Allen, P., Danisch, S., . . . Pohlmann, S. (2010).  
554 TMPRSS2 and TMPRSS4 facilitate trypsin-independent spread of influenza virus in Caco-2 cells.  
555 *J Virol*, 84(19), 10016-10025. doi:10.1128/JVI.00239-10

556 Boni, M. F., Lemey, P., Jiang, X., Lam, T. T., Perry, B. W., Castoe, T. A., . . . Robertson, D. L. (2020).  
557 Evolutionary origins of the SARS-CoV-2 sarbecovirus lineage responsible for the COVID-19  
558 pandemic. *Nat Microbiol*. doi:10.1038/s41564-020-0771-4

559 Bozzo, C. P., Nchioua, R., Volcic, M., Wettstein, L., Weil, T., Krüger, J., . . . Kirchhoff, F. (2020). IFITM  
560 proteins promote SARS-CoV-2 infection of human lung cells. *bioRxiv*, 2020.2008.2018.255935.  
561 doi:10.1101/2020.08.18.255935

562 Buchrieser, J., Dufloo, J., Hubert, M., Monel, B., Planas, D., Rajah, M. M., . . . Schwartz, O. (2020).  
563 Syncytia formation by SARS-CoV-2 infected cells. *bioRxiv*, 2020.2007.2014.202028.  
564 doi:10.1101/2020.07.14.202028

565 Cantuti-Castelvetri, L., Ojha, R., Pedro, L. D., Djannatian, M., Franz, J., Kuivanen, S., . . . Simons, M.  
566 (2020). Neuropilin-1 facilitates SARS-CoV-2 cell entry and provides a possible pathway into the  
567 central nervous system. *bioRxiv*, 2020.2006.2007.137802. doi:10.1101/2020.06.07.137802

568 Coutard, B., Valle, C., de Lamballerie, X., Canard, B., Seidah, N. G., & Decroly, E. (2020). The spike  
569 glycoprotein of the new coronavirus 2019-nCoV contains a furin-like cleavage site absent in  
570 CoV of the same clade. *Antiviral Res*, 176, 104742. doi:10.1016/j.antiviral.2020.104742

571 Daly, J. L., Simonetti, B., Antón-Plágaro, C., Kavanagh Williamson, M., Shoemark, D. K., Simón-Gracia,  
572 L., . . . Yamauchi, Y. (2020). Neuropilin-1 is a host factor for SARS-CoV-2 infection. *bioRxiv*,  
573 2020.2006.2005.134114. doi:10.1101/2020.06.05.134114

574 Davidson, A. D., Williamson, M. K., Lewis, S., Shoemark, D., Carroll, M. W., Heesom, K. J., . . . Matthews,  
575 D. A. (2020). Characterisation of the transcriptome and proteome of SARS-CoV-2 reveals a cell  
576 passage induced in-frame deletion of the furin-like cleavage site from the spike glycoprotein.  
577 *Genome Med*, 12(1), 68. doi:10.1186/s13073-020-00763-0

578 Edie, S., Zaghloul, N. A., Leitch, C. C., Klinedinst, D. K., Lebron, J., Thole, J. F., . . . Reeves, R. H. (2018).  
579 Survey of Human Chromosome 21 Gene Expression Effects on Early Development in Danio  
580 rerio. *G3 (Bethesda)*, 8(7), 2215-2223. doi:10.1534/g3.118.200144

581 Everitt, A. R., Clare, S., Pertel, T., John, S. P., Wash, R. S., Smith, S. E., . . . Kellam, P. (2012). IFITM3  
582 restricts the morbidity and mortality associated with influenza. *Nature*, 484(7395), 519-523.  
583 doi:10.1038/nature10921

584 Goldhill, D. H., Langat, P., Xie, H., Galiano, M., Miah, S., Kellam, P., . . . Barclay, W. S. (2019).  
585 Determining the Mutation Bias of Favipiravir in Influenza Virus Using Next-Generation  
586 Sequencing. *J Virol*, 93(2). doi:10.1128/JVI.01217-18

587 Goldhill, D. H., Te Velthuis, A. J. W., Fletcher, R. A., Langat, P., Zambon, M., Lackenby, A., & Barclay, W.  
588 S. (2018). The mechanism of resistance to favipiravir in influenza. *Proc Natl Acad Sci U S A*,  
589 115(45), 11613-11618. doi:10.1073/pnas.1811345115

590 Hanley, B., Naresh, K. N., Roufosse, C., Nicholson, A. G., Weir, J., Cooke, G. S., . . . Osborn, M. (2020).  
591 Histopathological findings and viral tropism in UK patients with severe fatal COVID-19: a post-  
592 mortem study. *Lancet Microbe*. doi:10.1016/S2666-5247(20)30115-4

593 Hoffmann, M., Kleine-Weber, H., & Pohlmann, S. (2020). A Multibasic Cleavage Site in the Spike  
594 Protein of SARS-CoV-2 Is Essential for Infection of Human Lung Cells. *Mol Cell*.  
595 doi:10.1016/j.molcel.2020.04.022

596 Hoffmann, M., Kleine-Weber, H., Schroeder, S., Kruger, N., Herrler, T., Erichsen, S., . . . Pohlmann, S.  
597 (2020). SARS-CoV-2 Cell Entry Depends on ACE2 and TMPRSS2 and Is Blocked by a Clinically  
598 Proven Protease Inhibitor. *Cell*, 181(2), 271-280 e278. doi:10.1016/j.cell.2020.02.052

599 Hoffmann, M., Mosbauer, K., Hofmann-Winkler, H., Kaul, A., Kleine-Weber, H., Kruger, N., . . .  
600 Pohlmann, S. (2020). Chloroquine does not inhibit infection of human lung cells with SARS-  
601 CoV-2. *Nature*. doi:10.1038/s41586-020-2575-3

602 Holshue, M. L., DeBolt, C., Lindquist, S., Lofy, K. H., Wiesman, J., Bruce, H., . . . Washington State -nCo,  
603 V. C. I. T. (2020). First Case of 2019 Novel Coronavirus in the United States. *N Engl J Med*,  
604 382(10), 929-936. doi:10.1056/NEJMoa2001191

605 Huang, I. C., Bailey, C. C., Weyer, J. L., Radoshitzky, S. R., Becker, M. M., Chiang, J. J., . . . Farzan, M.  
606 (2011). Distinct patterns of IFITM-mediated restriction of filoviruses, SARS coronavirus, and  
607 influenza A virus. *PLoS pathogens*, 7(1), e1001258. doi:10.1371/journal.ppat.1001258

608 Jabara, C. B., Jones, C. D., Roach, J., Anderson, J. A., & Swanstrom, R. (2011). Accurate sampling and  
609 deep sequencing of the HIV-1 protease gene using a Primer ID. *Proc Natl Acad Sci U S A*,  
610 108(50), 20166-20171. doi:10.1073/pnas.1110064108

611 Johnson, B. A., Xie, X., Kalveram, B., Lokugamage, K. G., Muruato, A., Zou, J., . . . Menachery, V. D.  
612 (2020). Furin Cleavage Site Is Key to SARS-CoV-2 Pathogenesis. *bioRxiv*,  
613 2020.2008.2026.268854. doi:10.1101/2020.08.26.268854

614 Kärber, G. (1931). Beitrag zur kollektiven Behandlung pharmakologischer Reihenversuche. *Naunyn-  
615 Schmiedebergs Archiv für experimentelle Pathologie und Pharmakologie*, 162(4), 480-483.  
616 doi:10.1007/BF01863914

617 Kim, Y. I., Kim, S. G., Kim, S. M., Kim, E. H., Park, S. J., Yu, K. M., . . . Choi, Y. K. (2020). Infection and  
618 Rapid Transmission of SARS-CoV-2 in Ferrets. *Cell Host Microbe*, 27(5), 704-709 e702.  
619 doi:10.1016/j.chom.2020.03.023

620 Klimstra, W. B., Tilston-Lunel, N. L., Nambulli, S., Boslett, J., McMillen, C. M., Gilliland, T., . . . Duprex,  
621 W. P. (2020). SARS-CoV-2 growth, furin-cleavage-site adaptation and neutralization using  
622 serum from acutely infected hospitalized COVID-19 patients. *J Gen Virol*.  
623 doi:10.1099/jgv.0.001481

624 Lau, S. Y., Wang, P., Mok, B. W., Zhang, A. J., Chu, H., Lee, A. C., . . . Chen, H. (2020). Attenuated SARS-  
625 CoV-2 variants with deletions at the S1/S2 junction. *Emerg Microbes Infect*, 9(1), 837-842.  
626 doi:10.1080/22221751.2020.1756700

627 Le Coupanec, A., Desforges, M., Meessen-Pinard, M., Dube, M., Day, R., Seidah, N. G., & Talbot, P. J.  
628 (2015). Cleavage of a Neuroinvasive Human Respiratory Virus Spike Glycoprotein by  
629 Proprotein Convertases Modulates Neurovirulence and Virus Spread within the Central  
630 Nervous System. *PLoS pathogens*, 11(11), e1005261. doi:10.1371/journal.ppat.1005261

631 Li, H., Bradley, K. C., Long, J. S., Frise, R., Ashcroft, J. W., Hartgroves, L. C., . . . Barclay, W. S. (2018).  
632 Internal genes of a highly pathogenic H5N1 influenza virus determine high viral replication in  
633 myeloid cells and severe outcome of infection in mice. *PLoS pathogens*, 14(1), e1006821.  
634 doi:10.1371/journal.ppat.1006821

635 Li, W., Moore, M. J., Vasilieva, N., Sui, J., Wong, S. K., Berne, M. A., . . . Farzan, M. (2003). Angiotensin-  
636 converting enzyme 2 is a functional receptor for the SARS coronavirus. *Nature*, 426(6965),  
637 450-454. doi:10.1038/nature02145

638 Lin, T. Y., Chin, C. R., Everitt, A. R., Clare, S., Perreira, J. M., Savidis, G., . . . Brass, A. L. (2013).  
639 Amphotericin B increases influenza A virus infection by preventing IFITM3-mediated  
640 restriction. *Cell Rep*, 5(4), 895-908. doi:10.1016/j.celrep.2013.10.033

641 Liu, Y., Gayle, A. A., Wilder-Smith, A., & Rocklov, J. (2020). The reproductive number of COVID-19 is  
642 higher compared to SARS coronavirus. *J Travel Med*, 27(2). doi:10.1093/jtm/taaa021

643 Liu, Z., Zheng, H., Lin, H., Li, M., Yuan, R., Peng, J., . . . Lu, J. (2020). Identification of common deletions  
644 in the spike protein of SARS-CoV-2. *J Virol.* doi:10.1128/JVI.00790-20

645 Long, J., Wright, E., Molesti, E., Temperton, N., & Barclay, W. (2015). Antiviral therapies against Ebola  
646 and other emerging viral diseases using existing medicines that block virus entry. *F1000Res*,  
647 4, 30. doi:10.12688/f1000research.6085.2

648 Ma, D., Chen, C. B., Jhanji, V., Xu, C., Yuan, X. L., Liang, J. J., . . . Ng, T. K. (2020). Expression of SARS-  
649 CoV-2 receptor ACE2 and TMPRSS2 in human primary conjunctival and pterygium cell lines  
650 and in mouse cornea. *Eye (Lond)*, 34(7), 1212-1219. doi:10.1038/s41433-020-0939-4

651 Mantlo, E., Bukreyeva, N., Maruyama, J., Paessler, S., & Huang, C. (2020). Antiviral activities of type I  
652 interferons to SARS-CoV-2 infection. *Antiviral Res*, 179, 104811.  
653 doi:10.1016/j.antiviral.2020.104811

654 Matsuyama, S., Nagata, N., Shirato, K., Kawase, M., Takeda, M., & Taguchi, F. (2010). Efficient  
655 activation of the severe acute respiratory syndrome coronavirus spike protein by the  
656 transmembrane protease TMPRSS2. *J Virol*, 84(24), 12658-12664. doi:10.1128/JVI.01542-10

657 Matsuyama, S., Nao, N., Shirato, K., Kawase, M., Saito, S., Takayama, I., . . . Takeda, M. (2020).  
658 Enhanced isolation of SARS-CoV-2 by TMPRSS2-expressing cells. *Proc Natl Acad Sci U S A*,  
659 117(13), 7001-7003. doi:10.1073/pnas.2002589117

660 McKay, P. F., Hu, K., Blakney, A. K., Samnuan, K., Brown, J. C., Penn, R., . . . Shattock, R. J. (2020). Self-  
661 amplifying RNA SARS-CoV-2 lipid nanoparticle vaccine candidate induces high neutralizing  
662 antibody titers in mice. *Nat Commun*, 11(1), 3523. doi:10.1038/s41467-020-17409-9

663 Millet, J. K., & Whittaker, G. R. (2014). Host cell entry of Middle East respiratory syndrome coronavirus  
664 after two-step, furin-mediated activation of the spike protein. *Proc Natl Acad Sci U S A*,  
665 111(42), 15214-15219. doi:10.1073/pnas.1407087111

666 Nao, N., Sato, K., Yamagishi, J., Tahara, M., Nakatsu, Y., Seki, F., . . . Takeda, M. (2019). Consensus and  
667 variations in cell line specificity among human metapneumovirus strains. *PLoS One*, 14(4),  
668 e0215822. doi:10.1371/journal.pone.0215822

669 Ogando, N. S., Dalebout, T. J., Zevenhoven-Dobbe, J. C., Limpens, R., van der Meer, Y., Caly, L., . . .  
670 Snijder, E. J. (2020). SARS-coronavirus-2 replication in Vero E6 cells: replication kinetics, rapid  
671 adaptation and cytopathology. *J Gen Virol*. doi:10.1099/jgv.0.001453

672 Ou, T., Mou, H., Zhang, L., Ojha, A., Choe, H., & Farzan, M. (2020). Hydroxychloroquine-mediated  
673 inhibition of SARS-CoV-2 entry is attenuated by TMPRSS2. *bioRxiv*, 2020.2007.2022.216150.  
674 doi:10.1101/2020.07.22.216150

675 Ou, X., Liu, Y., Lei, X., Li, P., Mi, D., Ren, L., . . . Qian, Z. (2020). Characterization of spike glycoprotein  
676 of SARS-CoV-2 on virus entry and its immune cross-reactivity with SARS-CoV. *Nat Commun*,  
677 11(1), 1620. doi:10.1038/s41467-020-15562-9

678 Park, J. E., Li, K., Barlan, A., Fehr, A. R., Perlman, S., McCray, P. B., Jr., & Gallagher, T. (2016). Proteolytic  
679 processing of Middle East respiratory syndrome coronavirus spikes expands virus tropism.  
680 *Proc Natl Acad Sci U S A*, 113(43), 12262-12267. doi:10.1073/pnas.1608147113

681 Richard, M., Kok, A., de Meulder, D., Bestebroer, T. M., Lamers, M. M., Okba, N. M. A., . . . Herfst, S.  
682 (2020). SARS-CoV-2 is transmitted via contact and via the air between ferrets. *Nat Commun*,  
683 11(1), 3496. doi:10.1038/s41467-020-17367-2

684 Sasaki, M., Uemura, K., Sato, A., Toba, S., Sanaki, T., Maenaka, K., . . . Sawa, H. (2020). SARS-CoV-2  
685 variants with mutations at the S1/S2 cleavage site are generated *<em>in vitro</em>* during  
686 propagation in TMPRSS2-deficient cells. *bioRxiv*, 2020.2008.2028.271163.  
687 doi:10.1101/2020.08.28.271163

688 Shang, J., Wan, Y., Luo, C., Ye, G., Geng, Q., Auerbach, A., & Li, F. (2020). Cell entry mechanisms of  
689 SARS-CoV-2. *Proc Natl Acad Sci U S A*. doi:10.1073/pnas.2003138117

690 Shi, G., Kenney, A. D., Kudryashova, E., Zhang, L., Hall-Stoodley, L., Robinson, R. T., . . . Yount, J. S.  
691 (2020). Opposing activities of IFITM proteins in SARS-CoV-2 infection. *bioRxiv*,  
692 2020.2008.2011.246678. doi:10.1101/2020.08.11.246678

693 Shirato, K., Kawase, M., & Matsuyama, S. (2013). Middle East respiratory syndrome coronavirus  
694 infection mediated by the transmembrane serine protease TMPRSS2. *J Virol*, 87(23), 12552-  
695 12561. doi:10.1128/JVI.01890-13

696 Shulla, A., Heald-Sargent, T., Subramanya, G., Zhao, J., Perlman, S., & Gallagher, T. (2011). A  
697 transmembrane serine protease is linked to the severe acute respiratory syndrome  
698 coronavirus receptor and activates virus entry. *J Virol*, 85(2), 873-882. doi:10.1128/JVI.02062-  
699 10

700 Simmons, G., Gosalia, D. N., Rennekamp, A. J., Reeves, J. D., Diamond, S. L., & Bates, P. (2005).  
701 Inhibitors of cathepsin L prevent severe acute respiratory syndrome coronavirus entry. *Proc  
702 Natl Acad Sci U S A*, 102(33), 11876-11881. doi:10.1073/pnas.0505577102

703 Sumner, R. P., Harrison, L., Touizer, E., Peacock, T. P., Spencer, M., Zuliani-Alvarez, L., & Towers, G. J.  
704 (2020). Disrupting HIV-1 capsid formation causes cGAS sensing of viral DNA. *EMBO J*, e103958.  
705 doi:10.15252/embj.2019103958

706 Wang, P., Lau, S.-Y., Deng, S., Chen, P., Mok, B. W.-Y., Zhang, A. J., . . . Chen, H. (2020). Pathogenicity,  
707 immunogenicity, and protective ability of an attenuated SARS-CoV-2 variant with a deletion  
708 at the S1/S2 junction of the spike protein. *bioRxiv*, 2020.2008.2024.264192.  
709 doi:10.1101/2020.08.24.264192

710 Wong, Y. C., Lau, S. Y., Wang To, K. K., Mok, B. W. Y., Li, X., Wang, P., . . . Chen, Z. (2020). Natural  
711 transmission of bat-like SARS-CoV-2PRRA variants in COVID-19 patients. *Clin Infect Dis*.  
712 doi:10.1093/cid/ciaa953

713 Wrensch, F., Winkler, M., & Pohlmann, S. (2014). IFITM proteins inhibit entry driven by the MERS-  
714 coronavirus spike protein: evidence for cholesterol-independent mechanisms. *Viruses*, 6(9),  
715 3683-3698. doi:10.3390/v6093683

716 Xia, S., Lan, Q., Su, S., Wang, X., Xu, W., Liu, Z., . . . Jiang, S. (2020). The role of furin cleavage site in  
717 SARS-CoV-2 spike protein-mediated membrane fusion in the presence or absence of trypsin.  
718 *Signal Transduct Target Ther*, 5(1), 92. doi:10.1038/s41392-020-0184-0

719 Xu-yang, Z., Pei-yu, B., Chuan-tao, Y., Wei, Y., Hong-wei, M., Kang, T., . . . Zhan-sheng, J. (2017).  
720 Interferon-Induced Transmembrane Protein 3 Inhibits Hantaan Virus Infection, and Its Single  
721 Nucleotide Polymorphism rs12252 Influences the Severity of Hemorrhagic Fever with Renal  
722 Syndrome. *Frontiers in Immunology*, 7(535). doi:10.3389/fimmu.2016.00535

723 Xu, Q. F., Zheng, Y., Chen, J., Xu, X. Y., Gong, Z. J., Huang, Y. F., . . . Lai, W. (2016). Ultraviolet A Enhances  
724 Cathepsin L Expression and Activity via JNK Pathway in Human Dermal Fibroblasts. *Chin Med  
725 J (Engl)*, 129(23), 2853-2860. doi:10.4103/0366-6999.194654

726 Zhang, Y. H., Zhao, Y., Li, N., Peng, Y. C., Giannoulatou, E., Jin, R. H., . . . Dong, T. (2013). Interferon-  
727 induced transmembrane protein-3 genetic variant rs12252-C is associated with severe  
728 influenza in Chinese individuals. *Nat Commun*, 4, 1418. doi:10.1038/ncomms2433

729 Zhao, X., Guo, F., Liu, F., Cuconati, A., Chang, J., Block, T. M., & Guo, J. T. (2014). Interferon induction  
730 of IFITM proteins promotes infection by human coronavirus OC43. *Proc Natl Acad Sci U S A*,  
731 111(18), 6756-6761. doi:10.1073/pnas.1320856111

732 Zhao, X., Sehgal, M., Hou, Z., Cheng, J., Shu, S., Wu, S., . . . Guo, J. T. (2018). Identification of Residues  
733 Controlling Restriction versus Enhancing Activities of IFITM Proteins on Entry of Human  
734 Coronaviruses. *J Virol*, 92(6). doi:10.1128/JVI.01535-17

735 Zhao, X., Zheng, S., Chen, D., Zheng, M., Li, X., Li, G., . . . Guo, J. T. (2020). LY6E Restricts the Entry of  
736 Human Coronaviruses, Including the Currently Pandemic SARS-CoV-2. *J Virol*.  
737 doi:10.1128/JVI.00562-20

738 Zheng, M., Zhao, X., Zheng, S., Chen, D., Du, P., Li, X., . . . Lin, H. (2020). Bat SARS-Like WIV1 coronavirus  
739 uses the ACE2 of multiple animal species as receptor and evades IFITM3 restriction via  
740 TMPRSS2 activation of membrane fusion. *Emerg Microbes Infect*, 9(1), 1567-1579.  
741 doi:10.1080/22221751.2020.1787797

742 Zhou, P., Yang, X. L., Wang, X. G., Hu, B., Zhang, L., Zhang, W., . . . Shi, Z. L. (2020). A pneumonia  
743 outbreak associated with a new coronavirus of probable bat origin. *Nature*, 579(7798), 270-  
744 273. doi:10.1038/s41586-020-2012-7

745 Zhou, Z., Wang, R., Yang, X., Lu, X. Y., Zhang, Q., Wang, Y. L., . . . Wang, H. (2014). The cAMP-responsive  
746 element binding protein (CREB) transcription factor regulates furin expression during human  
747 trophoblast syncytialization. *Placenta*, 35(11), 907-918. doi:10.1016/j.placenta.2014.07.017

748 Zhu, N., Zhang, D., Wang, W., Li, X., Yang, B., Song, J., . . . Research, T. (2020). A Novel Coronavirus  
749 from Patients with Pneumonia in China, 2019. *N Engl J Med*, 382(8), 727-733.  
750 doi:10.1056/NEJMoa2001017

751 Zhu, Y., Feng, F., Hu, G., Wang, Y., Yu, Y., Zhu, Y., . . . Zhang, R. (2020). The S1/S2 boundary of SARS-  
752 CoV-2 spike protein modulates cell entry pathways and transmission. *bioRxiv*,  
753 2020.2008.2025.266775. doi:10.1101/2020.08.25.266775

754 **Figure Legends**

755 **Figure 1. The SARS-CoV-2 spike contains a suboptimal polybasic furin cleavage site at the S1/S2 site.**

756 (A) Amino acid sequence alignment of coronavirus furin cleavage site mutants used in this  
757 study. Mutants with potential S1/S2 furin cleavage sites shown in shades of orange while  
758 mutants without furin cleavage sites shown in shades of blue.

759 (B) Syncytia formation due to overexpression of different coronavirus spike proteins in Vero  
760 E6 cells. Percentage indicates proportion of nuclei in each field which have formed clear  
761 syncytia. Statistical significance determined by one-way ANOVA with multiple comparisons  
762 against SARS-CoV-2 WT. \*\*\*\* indicates P value < 0.0001.

763 (C) Western blot analysis of concentrated lentiviral pseudotypes with different coronavirus  
764 spike proteins. Levels of lentiviral p24 antigen shown as loading control. Lentiviral  
765 pseudotypes labelled 'furin inhibitor' were generated in the presence of 5  $\mu$ M Decanoyl-RVKR-  
766 CMK, added 3 hours post-transfection.

767 (D) Western blot analysis of concentrated WT and  $\Delta$ CS SARS-CoV-2 viruses. Levels of  
768 nucleocapsid (N) protein shown as loading control.

769 **Figure 2. The furin cleavage site of SARS-CoV-2 mediates entry into mucosal epithelial and primary**  
770 **human airway cells**

771 (A) SARS-CoV-2 competition assay growth curve between WT and  $\Delta$ CS virus in Vero E6 and  
772 Caco-2 cells. Cells infected at an MOI of 0.1. Starting inoculum ratio shown on the left-hand  
773 bar while proportions of virus as determined by deep sequencing at 72 hours post-inoculation  
774 shown on the right. Virus titres determined by plaque assay at 72 hours post-inoculation  
775 shown in superimposed white data points. All results indicate triplicate repeats.

776 (B) SARS-CoV-2 competition assay growth curve between WT and  $\Delta$ CS virus in human airway  
777 epithelial cells (HAEs). Cells infected at an MOI of 0.1. Starting inoculum ratio shown at time  
778 0, proportions of virus determined by deep sequencing. All time points taken from triplicate  
779 repeats. Virus replication determined by plaque assay and shown as imposed white data  
780 points.

781 (C) Head to head replication kinetics of clonal WT and  $\Delta$ CS viruses in Calu-3 human lung cells.  
782 Cells infected at an MOI of 0.1. All time points taken from triplicate repeats. Virus replication  
783 determined by plaque assay. Statistics determined by Student's t-test on log transformed  
784 data. \*\*\*,  $0.001 \geq P > 0.0001$ ; \*\*\*\*,  $P \leq 0.0001$ .

785 (D,E,F) Entry of lentiviral pseudotypes (PV) containing different viral glycoproteins into 293T-  
786 ACE2 (D), Caco-2 (E) and Calu-3 (F) cells. Cells transduced with different PV and lysed 48 hours  
787 later and analysed by firefly luciferase luminescence. All assays performed in triplicate.  
788 Statistics determined by one-way ANOVA on Log-transformed data (after determining log  
789 normality by the Shapiro-Wilk test and QQ plot.) \*,  $0.05 \geq P > 0.01$ ; \*\*,  $0.01 \geq P > 0.001$ ; \*\*\*,  
790  $0.001 \geq P > 0.0001$ ; \*\*\*\*,  $P \leq 0.0001$ .

791 (G,H) Relative entry of PV grown in the absence or presence of furin inhibitor (5  $\mu$ M Decanoyl-  
792 RVKR-CMK) into 293T-ACE2 (G) or Caco-2 (H) cells. Untreated PV normalised to an RLU of 1.  
793 Statistics determined by multiple t-tests. All assays performed in triplicate. \*\*,  $0.01 \geq P >$   
794  $0.001$ .

795 **Figure 3. The furin cleavage site of SARS-CoV-2 spike allows more efficient serine-protease  
796 dependent entry into airway cells.**

797 (A,B,C) Inhibition of entry of lentiviral pseudotypes into (A) 293T-ACE2, (B) Caco-2 or (C) Calu-  
798 3 cells by the serine protease inhibitor, camostat (green bars) or the cathepsin inhibitor, E64-  
799 d (Purple bars). All data normalised to no drug control (black bars). Statistics determined by  
800 two-way ANOVA with multiple comparisons against the no drug control. \*, 0.05  $\geq$  P > 0.01; \*\*,  
801 0.01  $\geq$  P > 0.001; \*\*\*, 0.001  $\geq$  P > 0.0001; \*\*\*\*, P  $\leq$  0.0001.  
  
802 (D) Replication kinetics of SARS-CoV-2 WT and  $\Delta$ CS viruses in HAE cells. Cells were pretreated  
803 with control media or media containing camostat for 1 hour then infected at an MOI of 0.1.  
804 Statistics were determined by one-way ANOVA with multiple comparisons on log transformed  
805 data. Black asterisks indicate statistical significance between no drug controls of WT and  $\Delta$ CS  
806 while coloured asterisks indicate significance between no drug control or camostat. \*, 0.05  $\geq$   
807 P > 0.01; \*\*, 0.01  $\geq$  P > 0.001; \*\*\*, 0.001  $\geq$  P > 0.0001; \*\*\*\*, P  $\leq$  0.0001.  
  
808 (E-H) Gene expression of select SARS-CoV-2 entry factors in (E) 293T-ACE2, (F) Caco-2, (G)  
809 Calu-3 or (H) HAEs. Gene expression determined by qRT-PCR and normalised to  $\beta$ -actin.

810 **Figure 4. The efficient furin cleavage site-dependent entry of SARS-CoV-2 is due to TMPRSS2 and**  
811 **allows for subsequent escape from IFITM3.**

812 (A) Relative lentiviral pseudotype (PV) entry into 293T cells expressing ACE2-FLAG with or  
813 without co-expression of TMPRSS2. Entry into cells not transfected with TMPRSS2 normalised  
814 to 1. Statistics determined by multiple t-tests. \*\*\*\*, P  $\leq$  0.0001.  
  
815 (B-D) Relative PV entry into (D) 293T-ACE2, (E) Caco-2 or (F) Calu-3 cells pretreated with  
816 Amphotericin B (pink bars). Entry into untreated cells normalised to 1 (black bars). Statistics  
817 determined by multiple t-tests. \*, 0.05  $\geq$  P > 0.01; \*\*, 0.01  $\geq$  P > 0.001  
  
818 (E) Relative PV entry into 293T cells overexpressing ACE2-FLAG and TMPRSS2, with or without  
819 IFITM3. Entry into cells not transfected with IFITM3 normalised to 1 (black bars). Statistics  
820 determined by multiple t-tests. \*\*, 0.01  $\geq$  P > 0.001; \*\*\*, 0.001  $\geq$  P > 0.0001; \*\*\*\*, P  $\leq$  0.0001.

821 (F) Replication kinetics of SARS-CoV-2 WT and  $\Delta$ CS viruses in HAE cells. Cells were pretreated  
822 with control media or media containing amphotericin B for 1 hour then infected at an MOI of  
823 0.1. Statistics were determined by one-way ANOVA with multiple comparisons on log  
824 transformed data. Black asterisks indicate statistical significance between no drug controls of  
825 WT and  $\Delta$ CS while coloured asterisks indicate significance between no drug control or  
826 amphoB. DMSO controls were the same as from Figure 3D. \*, 0.05  $\geq$  P  $>$  0.01; \*\*, 0.01  $\geq$  P  $>$   
827 0.001; \*\*\*, 0.001  $\geq$  P  $>$  0.0001; \*\*\*\*, P  $\leq$  0.0001.

828 **Figure 5. The furin cleavage site of SARS-CoV-2 allows for efficient replication and transmission in a**  
829 **ferret model**

830 (A, B) Head to head transmission experiment of SARS-CoV-2 mix of WT and  $\Delta$ CS in ferrets.  
831 In each group four individually housed donor ferrets were infected with X pfu of either  
832 WT or  $\Delta$ CS SARS-CoV-2. One day post-inoculation naïve contact ferrets were added to  
833 each donor ferret. Ferrets were sampled by nasal wash daily and direct contact (A) and  
834 contact (B) ferret virus titres were determined by E gene qPCR. Statistics were determined  
835 by multiple t tests of the log transformed E gene copy numbers between each group. \*,  
836 0.05  $\geq$  P

837 (C) Competition transmission experiment of SARS-CoV-2 mix of WT and  $\Delta$ CS in ferrets.  
838 Four individually housed donor ferrets were infected with  $10^5$  pfu of virus mix containing  
839  $\sim$ 70%  $\Delta$ CS and  $\sim$ 30% WT. One day post-inoculation naïve contact ferrets were added to  
840 each donor ferret. Ferrets were sampled by nasal wash daily and virus titres were  
841 determined by E gene qPCR. For donors on day 2, 3, 5, 6 and 8, and for contacts on day 3,  
842 6, 8 and 9 viral RNA across the S1/S2 cleavage site was deep sequenced. Where  
843 sequencing data was obtained bars showing the ratio of WT and deletion are shown.

844 **Supplementary Figure Legends**

845 **Supplementary Figure S1. Expression of transfected ACE2, TMPRSS2 and IFITM3**

846 (A) Expression of TMPRSS2 and ACE2-FLAG in 293T cells shown by western blot (from Figure  
847 4A).

848 (B) Expression of IFITM3 in 293T cells shown by western blot (from Figure 4G)

849 **Supplementary Figure S2. Ferret head-to-head transmission experiment addition shedding data  
850 and clinical data**

851 (A, B) Infectious virus titres of WT (orange) or ΔCS (blue) taken from donor ferret (A) and direct  
852 contact ferret (B) nasal washes as determined by TCID<sub>50</sub>. Dotted line indicates limit of  
853 detection of infectious virus.

854 (C) Microneutralisation assay showing ferret post-infection serology. Threshold of detection  
855 was a neutralisation titre of 10 (dotted line). Serum taken 14 days post-infection.

856 (D) Changes in donor and direct contact ferret body weights during the duration of the  
857 infection.

858 (E) Changes in donor and direct contact ferret body temperatures during the duration of the  
859 infection.

860 **Supplementary Figure S3. Ferret competition transmission experiment clinical data.**

861 (A, B) Changes in donor (A) and direct contact (B) ferret body temperatures during the  
862 duration of the infection.

863 (C) Changes in ferret body weight (in percentage) during the duration of the infection.

864 (D) Microneutralisation assay showing ferret post-infection serology. Threshold of detection  
865 was a neutralisation titre of 10 (dotted line). Serum taken 14 days post-infection.

866 **Supplementary Table 1. S1/S2 cleavage site deletions reported following viral passage in cell**

867 **culture or from clinical samples.**

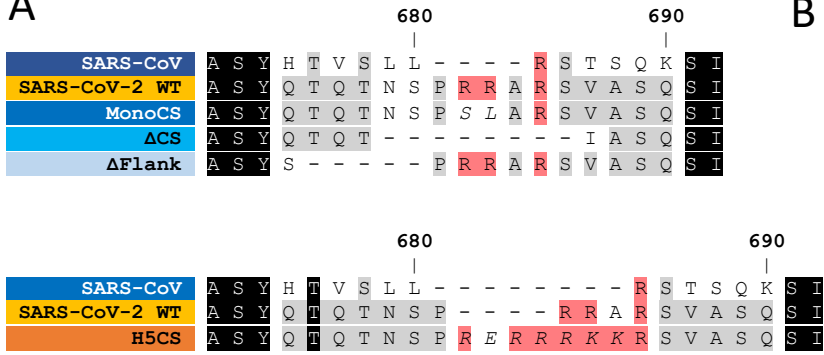
868 **Supplementary Table 2. Post-mortem samples sequenced for S1/S2 cleavage site deletions.**

869

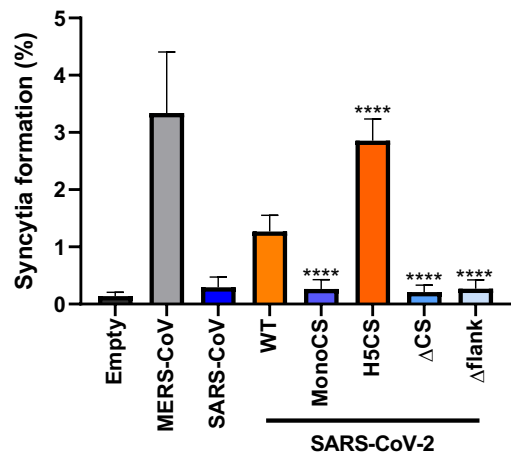
870

**Figure 1: the SARS-CoV-2 spike contains a suboptimal polybasic furin cleavage site at the S1/S2 site.**

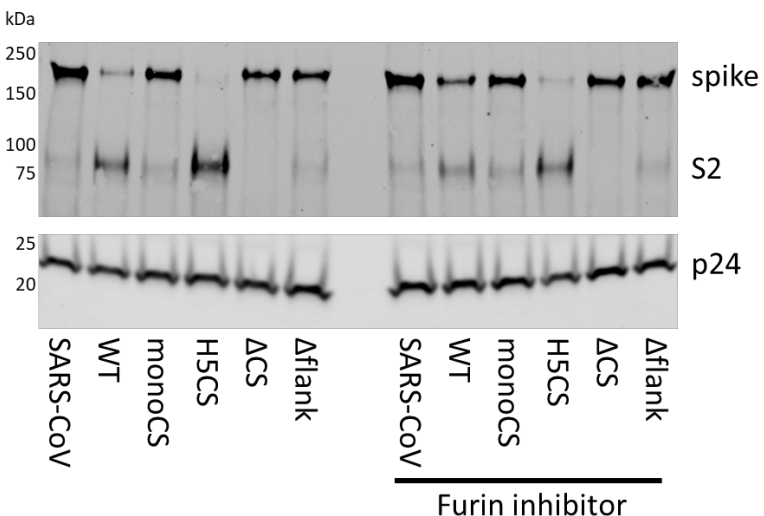
**A**



**B**



**C**



**D**

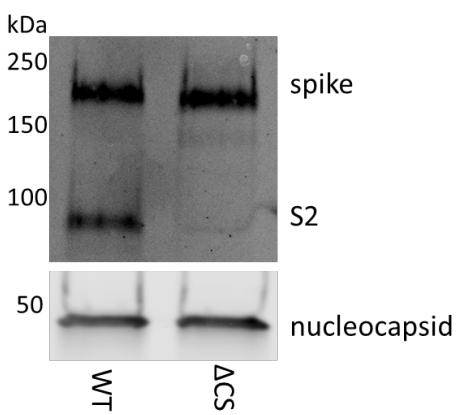


**Figure 2: the furin cleavage site of SARS-CoV-2 mediates entry into mucosal epithelial and primary human airway cells**

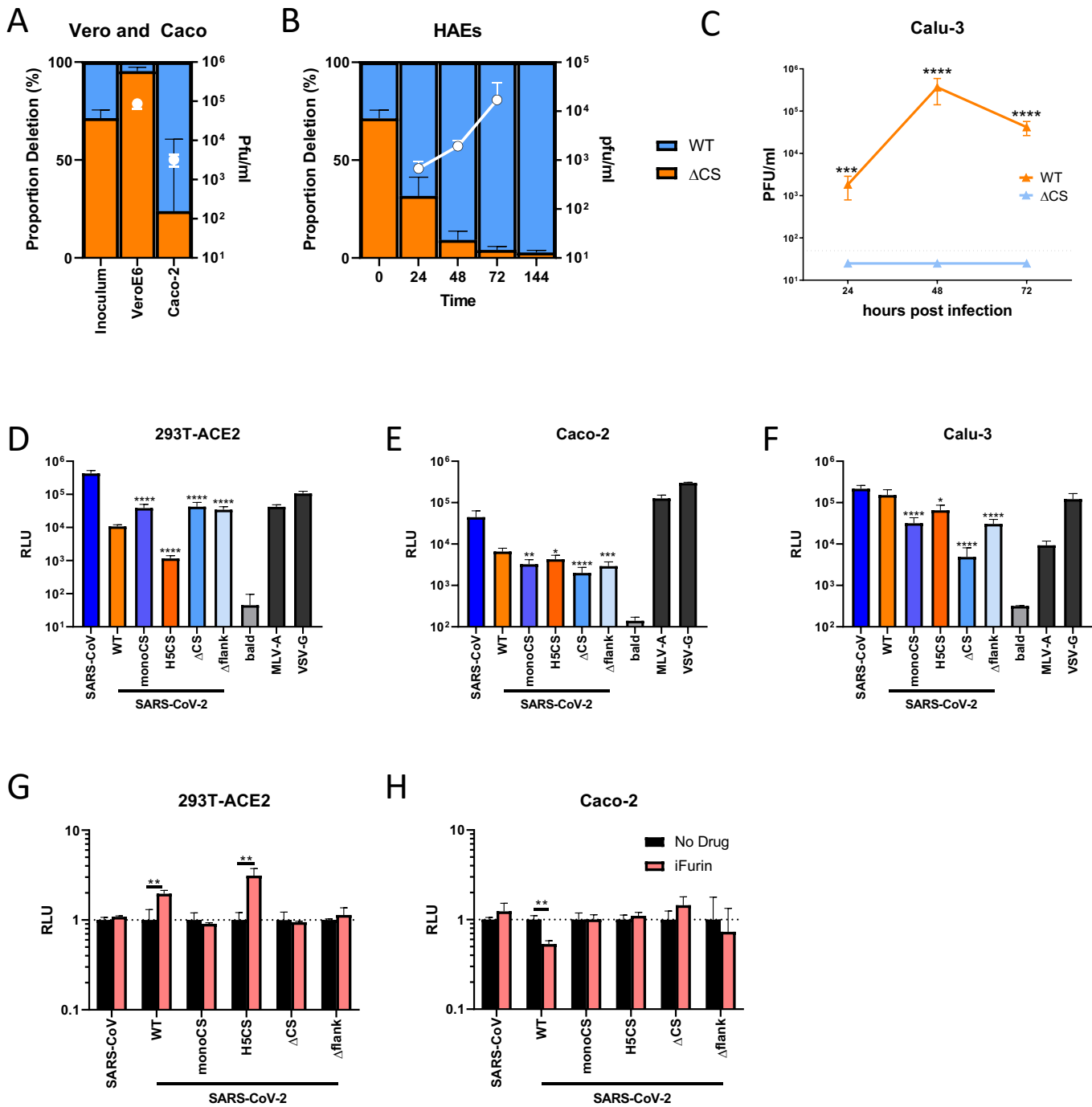
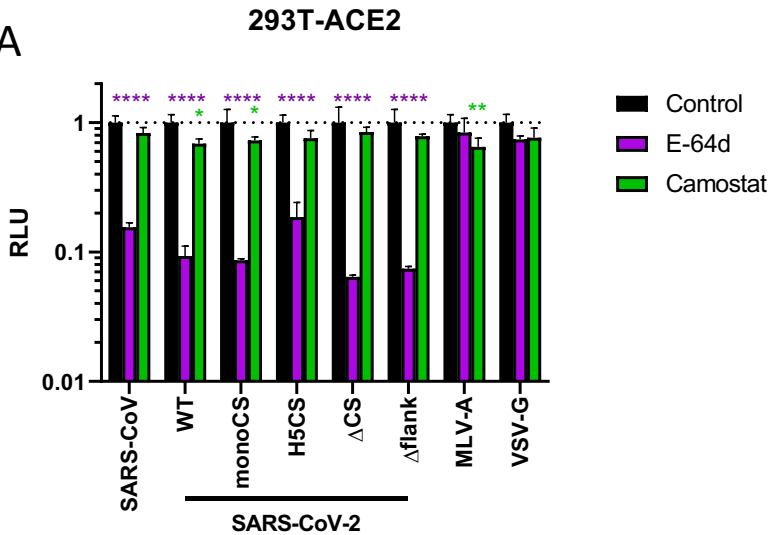
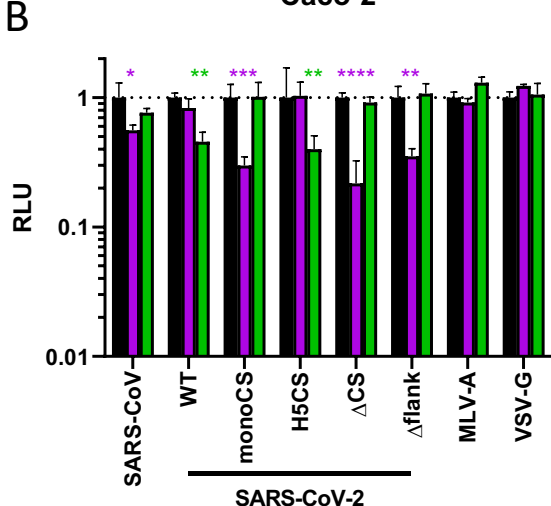


**Figure 3: The furin cleavage site of SARS-CoV-2 spike allows more efficient serine-protease dependent entry into airway cells**

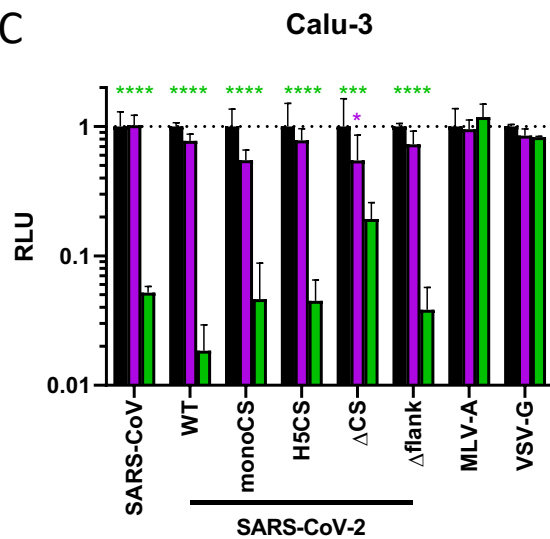
**A**



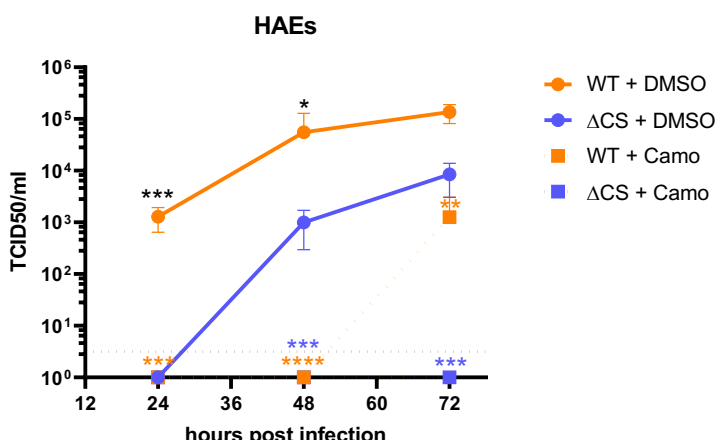
**B**



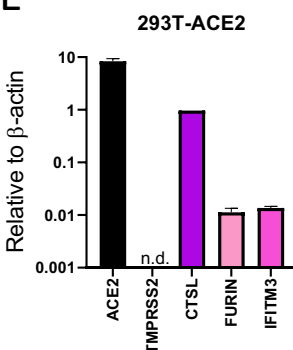
**C**



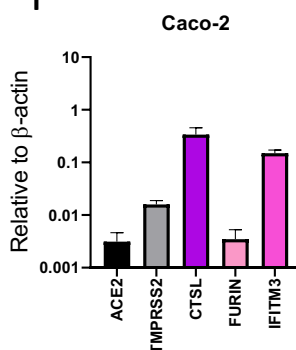
**D**



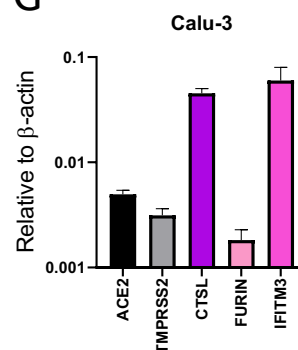
**E**



**F**



**G**



**H**

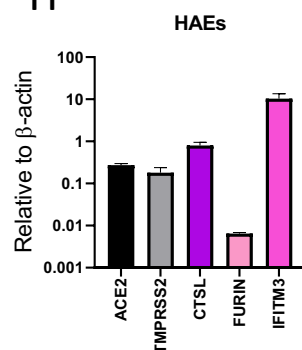


**Figure 4: The efficient furin cleavage site-dependent entry of SARS-CoV-2 is due to TMPRSS2 and allows for subsequent escape from IFITM3.**

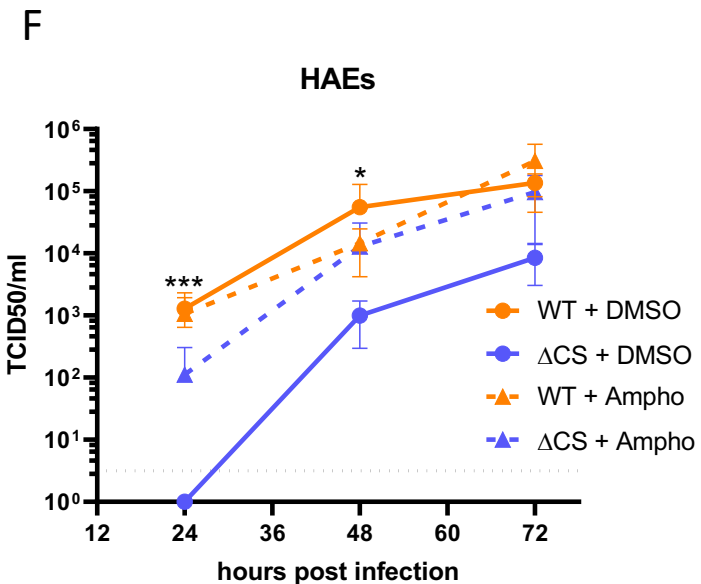
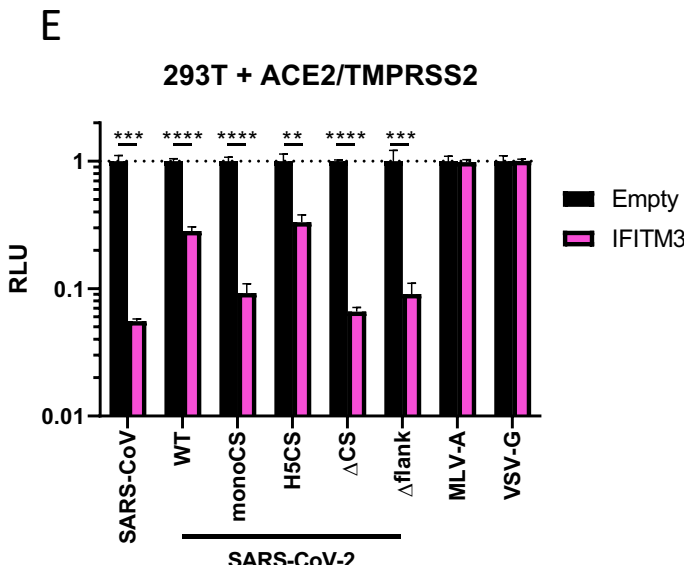
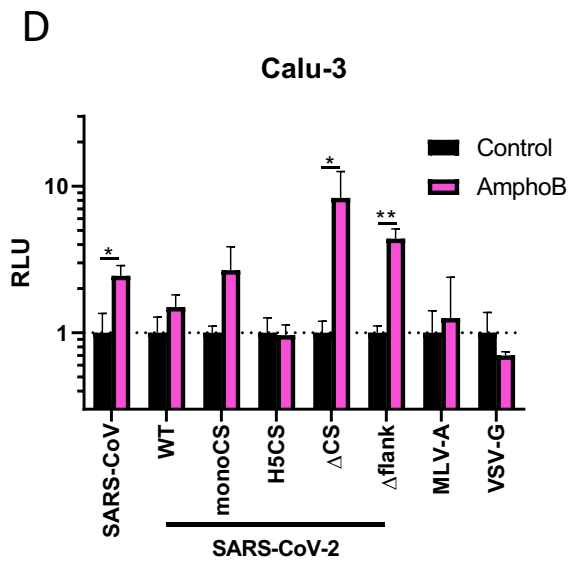
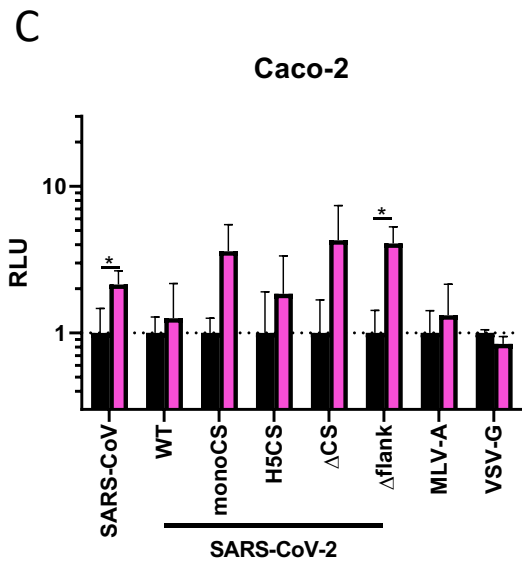
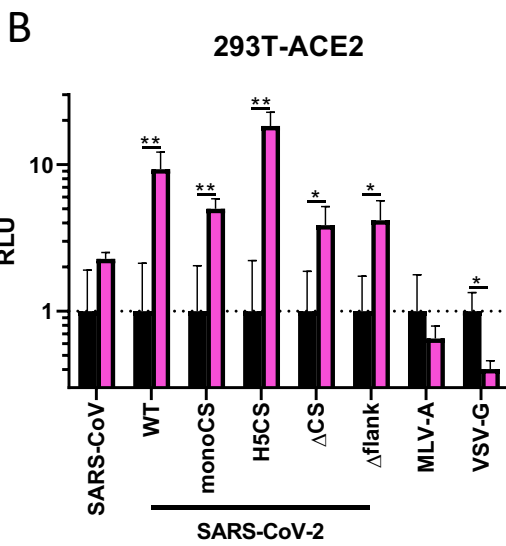
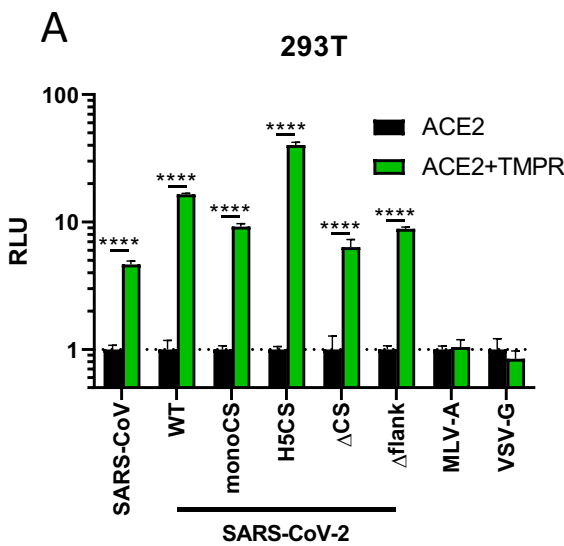
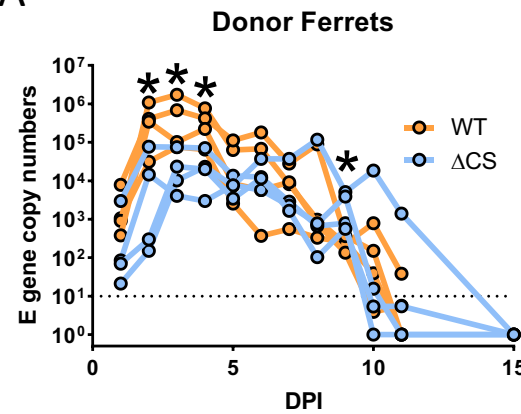
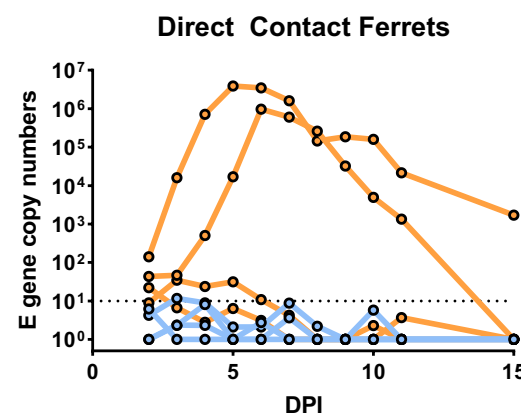


**Figure 5: The furin cleavage site of SARS-CoV-2 allows for efficient replication and transmission in a ferret model**

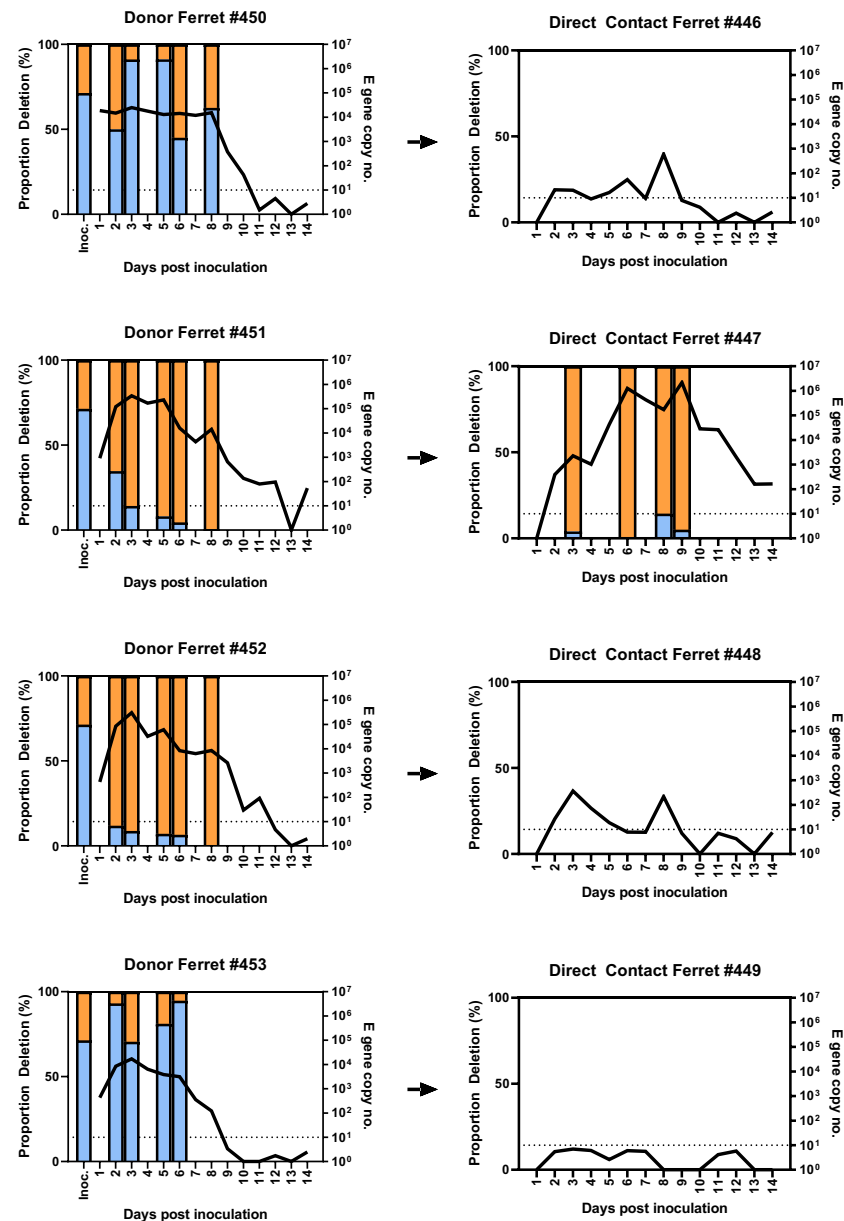
**A**



**B**

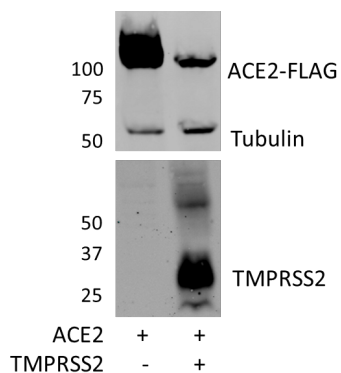


**C**

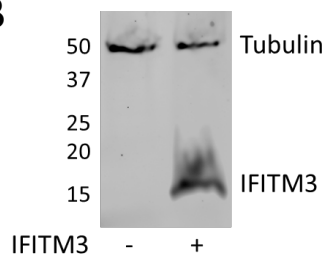


## Supplementary Figure S1 – Expression of transfected ACE2, TMPRSS2 and IFITM3

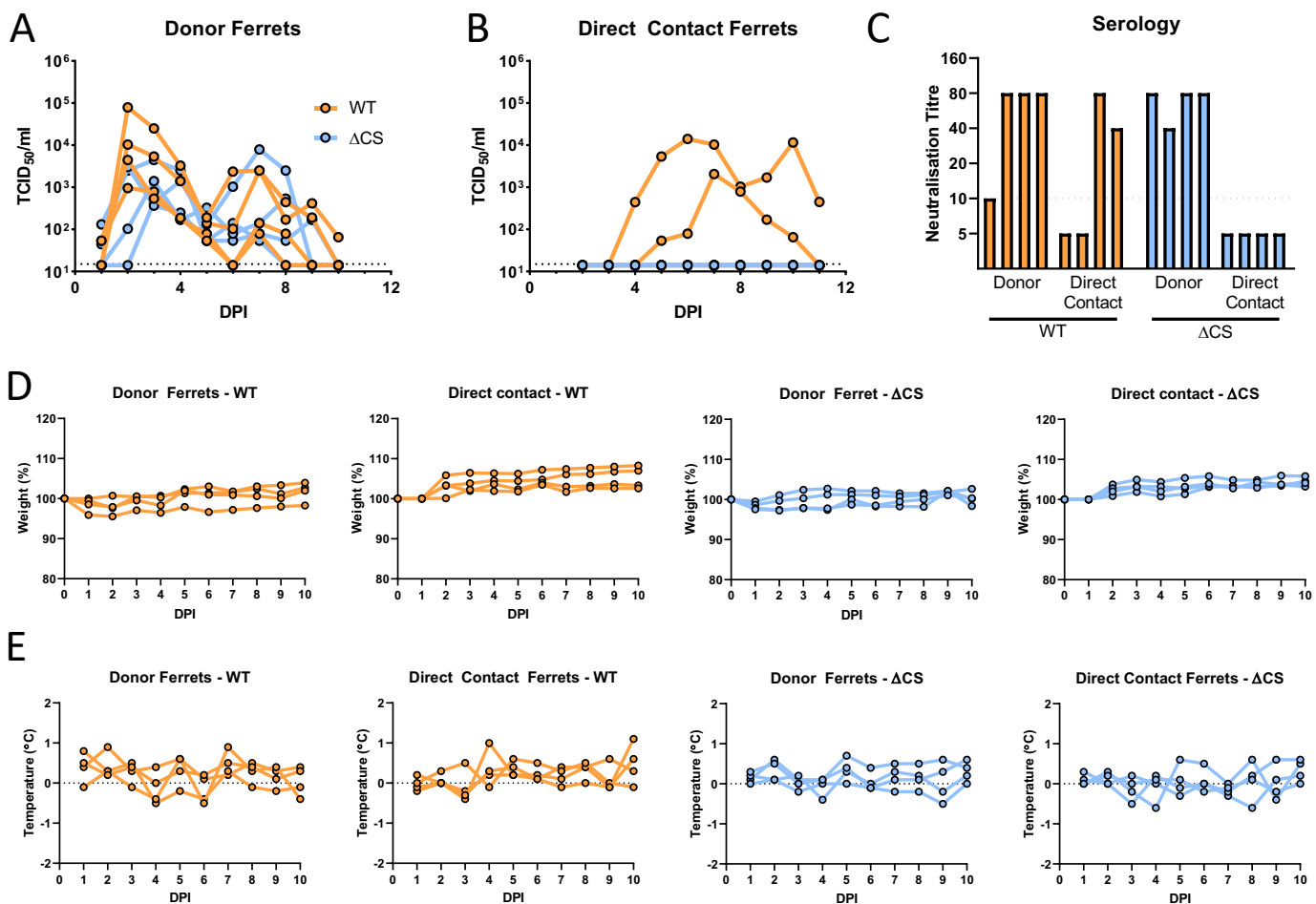
A



B



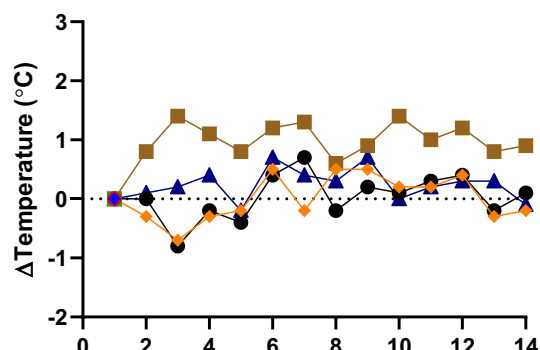
## Supplementary Figure S2 – Ferret head-to-head transmission experiment addition shedding data and clinical data



Supplementary Figure S3 – Ferret competition transmission experiment clinical data

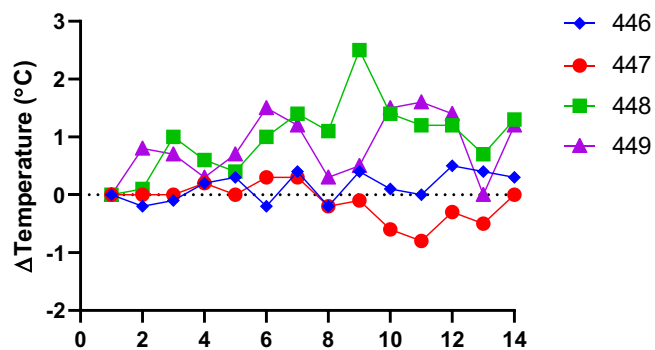
A

Donor ferrets



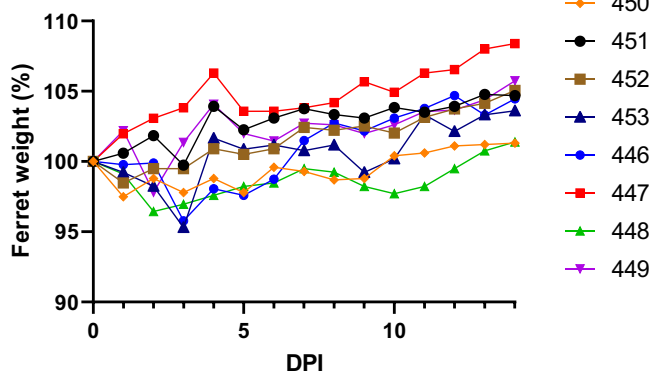
B

Direct contact ferrets



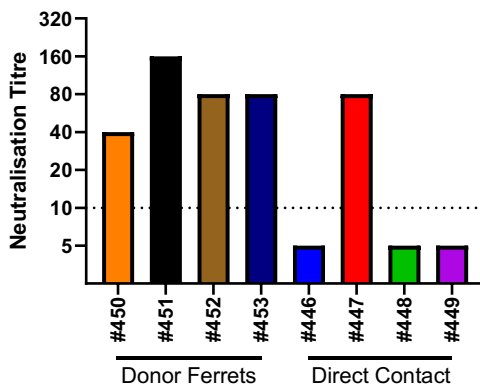
C

Ferret weight loss



D

Ferret Serology



**Supplementary Table 1. S1/S2 cleavage site deletions reported following viral passage in cell culture or from clinical samples.**

	670	680	690	
<i>SARS-CoV-2 WT</i>				
	PIGAGICASYQTQTNS	<span style="background-color: red;">PRRARSVASQSIIAYTM</span>		
<b>Vero-Passaged</b>				
ΔCT	PIGAGICASYQTQT-----	IASQSIIAYTM		
ΔFlank	PIGAGICASY-----S	<span style="background-color: red;">PRRARSVASQSIIAYTM</span>		
Ogando et al.; Wong et al.; Sasaki et al.	PIGAGICASYQTQT-----	SQSIIAYTM		
Liu et al.; Wong et al.	PIGAGICASYQTQT-----	SVASQSIIAYTM		
Sasaki et al.	PIGAGICASYQTQTNS	<span style="background-color: red;">PRRARSVA---IIAYTM</span>		
Sasaki et al.; Zhu et al.	PIGAGICASYQTQTNSPR	-----QSIIAYTM		
<b>Post Mortem</b>				
OS5 – Heart	PIGAGICASYQTQTNS	<span style="background-color: red;">PRRARSVA---IAYTM</span>		
OS19-1 – Spleen	PIGAG-----NS	<span style="background-color: red;">PRRARSVASQSIIAYTM</span>		
OS19-2 – Spleen	PIGAGICASYQTQTNS	-----SQSIIAYTM		
<b>Clinical Isolates</b>				
England/20238034404/2020	PIGAGICASYQTQT-----	IASQSIIAYTM		
USA/MO-WUSTL069/2020	PIGAGICASYQTQ-----	QSIIAYTM		

**Supplementary Table 2. Post-mortem samples sequenced for S1/S2 cleavage site deletions.**

Sample type	Post mortem case	Ct value by E gene qRT-PCR	Deletions detected?
bone marrow	PM3	30.2	N
brain	PM2	25.4	N
heart	PM1	18.8	N
	PM2	21.2	Y - OS5
	PM6	17.7	N
ileum	PM1	31.3	N
	PM2	28.3	N
	PM4	31.7	N
	PM6	25.1	N
kidney	PM4	31.4	N
	PM6	25.8	N
lung	PM1	30.2	N
	PM3	19.7	N
	PM6	11.5	N
nasal	PM1	32.1	N
	PM3	30.8	N
	PM4	23.8	N
spleen	PM3	28.5	Y - OS19-1, OS19-2
tongue	PM3	24.3	N
	PM4	24.3	N
	PM6	21.9	N
trachea	PM1	32.7	N
	PM3	19.9	N
	PM4	23.5	N